Mössbauer spectroscopy for heavy elements: a relativistic benchmark study of mercury

Knecht, S.; Fux, S.; van Meer, R.; Visscher, L.; Reiher, M.; Saue, T.

published in
Theoretical Chemistry Accounts
2011

DOI (link to publisher)
10.1007/s00214-011-0911-2

document version
Publisher's PDF, also known as Version of record

Theor Chem Acc (2011) 129:631–650
DOI 10.1007/s00214-011-0911-2

REGULAR ARTICLE

Mössbauer spectroscopy for heavy elements: a relativistic benchmark study of mercury

Stefan Knecht · Samuel Fux · Robert van Meer · Lucas Visscher · Markus Reiher · Trond Saue

Received: 9 November 2010 / Accepted: 14 February 2011 / Published online: 11 March 2011

Abstract The electrostatic contribution to the Mössbauer isomer shift of mercury for the series HgF_n ($n = 1, 2, 4$) with respect to the neutral atom has been investigated in the framework of four- and two-component relativistic theory. Replacing the integration of the electron density over the nuclear volume by the contact density (that is, the electron density at the nucleus) leads to a 10% overestimation of the isomer shift. The systematic nature of this error suggests that it can be incorporated into a correction factor, thus justifying the use of the contact density for the calculation of the Mössbauer isomer shift. The performance of a large selection of density functionals for the calculation of contact densities has been assessed by comparing with finite-field four-component relativistic coupled-cluster with single and double and perturbative triple excitations [CCSD(T)] calculations. For the absolute contact density of the mercury atom, the Density Functional Theory (DFT) calculations are in error by about 0.5%, a result that must be judged against the observation that the change in contact density along the series HgF_n ($n = 1, 2, 4$), relevant for the isomer shift, is on the order of 50 ppm with respect to absolute densities. Contrary to previous studies of the ^{57}Fe isomer shift (F Neese, Inorg Chim Acta 332:181, 2002), for mercury, DFT is not able to reproduce the trends in the isomer shift provided by reference data, in our case CCSD(T) calculations, notably the non-monotonous decrease in the contact density along the series HgF_n ($n = 1, 2, 4$). Projection analysis shows the expected reduction of the $6s_{1/2}$ population at the mercury center with an increasing number of ligands, but also brings into light an opposing effect, namely the increasing polarization of the $6s_{1/2}$ orbital due to increasing effective charge of the mercury atom, which explains the non-monotonous behavior of the contact density along the series. The same analysis shows increasing covalent contributions to bonding along the series with the effective charge of the mercury atom reaching a maximum of around $+2$ for HgF_4 at the DFT level, far from the formal charge $+4$ suggested by the oxidation state of this recently observed species. Whereas the geometries for the linear HgF_2 and square-planar HgF_4 molecules were taken from previous computational studies, we optimized the equilibrium distance of HgF at the four-component Fock-space CCSD/aug-cc-pVQZ level, giving spectroscopic constants $r_e = 2.007$ Å and $\omega_e = 513.5$ cm^{-1}.

Dedicated to Professor Pekka Pyykkö on the occasion of his 70th birthday and published as part of the Pyykkö Festschrift Issue.

Electronic supplementary material The online version of this article (doi:10.1007/s00214-011-0911-2) contains supplementary material, which is available to authorized users.

S. Knecht
Institute de Chimie de Strasbourg, CNRS et Université de Strasbourg, Laboratoire de Chimie Quantique, 4 rue Blaise Pascal, 67070 Strasbourg, France

S. Fux · M. Reiher
ETH Zurich, Laboratorium für Physikalische Chemie, Wolfgang-Pauli-Strasse 10, 8093 Zurich, Switzerland

R. van Meer · L. Visscher
Amsterdam Center for Multiscale Modeling, VU University Amsterdam, De Boelelaan 1083, 1081 HV Amsterdam, The Netherlands

T. Saue (✉)
Laboratoire de Chimie et Physique Quantique (CNRS UMR 5626), IRSAMC, Université Paul Sabatier, 118 Route de Narbonne, 31062 Toulouse cedex, France
e-mail: trond.saue@irsamc.ups-tlse.fr

Keyword Mössbauer spectroscopy · Relativistic quantum chemistry · Density functional theory · Coupled cluster · Contact density · Mercury compounds · Picture change effects

1 Introduction

Molecular properties of heavy element compounds are known to be affected by relativistic effects [1–3], especially if they are probed at a heavy atomic nucleus. One such property is the contact density, i.e., the electron (number) density at the center of an atomic nucleus. The contact density can be related to the chemical isomer shift [4–9] that is observed in Mössbauer spectra if the frequency of the γ-radiation absorbed by a nucleus (absorber nucleus) in a solid is not equal to the one emitted by a source nucleus of the same element. Rephrased in terms of relative energy, the energy difference between ground and excited states of the absorbing compound is different from that of the emitting compound. This relative energy shift is usually expressed in terms of the speed of the source relative to the absorber which creates the Doppler shift necessary to bring the emitter and absorber into resonance.

Each of these energies can be calculated as the electrostatic interaction between electronic and nuclear charge distributions in the particular states. However, usually some well-investigated approximations are made in order to reduce the energies to descriptors like the contact density. First of all, one assumes that the change in electronic charge distribution for the ground and excited nuclear states, which are characterized by *nuclear* charge distributions of different extension, can be neglected. Then, it is assumed that the electronic charge distribution is approximately constant over the size of the atomic nucleus and hence can be described by a single value, namely by the contact density. For a homogeneously charged, spherical nucleus, one then obtains a simplified expression for the energy difference ΔE_{IS} due to the isomer shift (IS),

$$\Delta E_{\mathrm{IS}} = \frac{2\pi}{5} Z \left[n^A(0) - n^S(0) \right] \left(R^{\star^2} - R_0^2 \right), \qquad (1)$$

where $n(0)$ denotes the contact electron density at the atomic nucleus of absorber A and source S, while $R^\star$ and R_0 are the nuclear radii in the excited and ground states, respectively. Z is the nuclear charge.

The usual point charge approximation of the nuclear density in the determination of the electronic density should be carefully examined in the calculation of contact densities. In non-relativistic theory, this approximation results in a cusp of the electron density at the position of the nuclei [10]. In relativistic theory, the electron density shows a weak (integrable) singularity at the nucleus. This limiting short-range behavior is, however, an artifact of the simple point charge model and is radically different for the more physical model of an extended nucleus. In the relativistic case, it is already common to introduce an extended-nucleus model [11–14] because this facilitates the use of Gaussian type orbitals (GTOs). GTOs have zero slope at the nucleus, which is consistent with the exact solutions for extended-nuclear models [15–18] in both non-relativistic and relativistic theory. This feature thus makes GTOs a natural expansion set for relativistic orbitals for which one may rely on well-established basis sets augmented by steep functions (as e.g., demonstrated recently for contact densities at iron nuclei [18]). By employing an extended-nucleus model, one may also go beyond the contact density approximation and explicitly calculate the change in nucleus–electron interaction corresponding to the nuclear transition measured in Mössbauer spectroscopy. This approach has been pursued by Filatov and co-workers [19–23] who introduce a difference in radius between the ground- and excited state nucleus as a finite perturbation that can be used to numerically differentiate the electronic energy. An added advantage is that such a finite difference scheme also works for methods for which it is difficult to obtain the relaxed density directly.

A more pragmatic approach, that works well for light elements, is based on the fact that the errors in the density arising from the approximation of the nucleus by a point charge model and by calculating the wave function in a non-relativistic framework, are almost exclusively atomic in nature. This feature makes it possible to derive corrections that scale non-relativistic contact densities, calculated with a GTO basis set and a point nucleus model, towards the true values. Such a useful pragmatic approach to the isomer shift has been suggested by Neese [24, 25] who employed non-relativistic density functional theory to capture valence-shell effects on the contact density, while the difficult-to-capture atomic contributions were absorbed in fit parameters upon parametrization against experimental results.

Although tin and especially iron nuclei are the most prominent Mössbauer nuclei in practice, we focus here on mercury, which is also Mössbauer active but for which there are much less experimental data available [26–31] (see Refs. [32–34] for additional spectroscopic properties of Hg in mercury compounds). Interestingly though, γ-ray fluorescence was first detected in liquid mercury [35, 36]. Mercury compounds feature two advantages: (1) they are prone to relativistic effects so that the reliability of different relativistic Hamiltonians can be thoroughly assessed and (2) they are usually closed-shell molecules so that highly accurate single-reference electron correlation methods can be employed, which allow us to assess different electronic structure methods for such closed-shell species.

In this work, we therefore focus on relativistic calculations of the mercury contact density in the atom as well as in fluorides of mercury. Among the mercury fluorides, which have been studied for various practical reasons [37], the tetrafluoride HgF_4 has in particular attracted attention in recent years [38, 39] since its theoretical prediction in 1993 [40]. This compound was discovered by matrix spectroscopy [41, 42], but has not yet been obtained in macroscopic yields. However, once this would have been accomplished, a solid sample of this material may be subjected to γ-radiation in a Mössbauer experiment in order to determine the oxidation state of Hg in HgF_4. This can then clarify a theoretical prediction by Pyykkö et al. [43] who assigned an extraordinarily high oxidation state of +IV to Hg (considering the fact that the common oxidation state of Hg in chemical compounds is only +II).

This paper is organized as follows: In the Theoretical section, we will first examine the validity of the contact density approximation in relativistic finite nucleus calculations, then discuss the calculation of the contact density in the four-component relativistic formulation, and finally the interpretation of calculated densities in terms of atomic contributions via a projection analysis. We then provide Computational Details about the calculations before embarking on the results in Sect. 4.

2 Theoretical considerations

2.1 Validity of the contact density approximation

The calculation of the Mössbauer isomer shift via calculated contact densities requires a number of approximations [44]. In the traditional approach [45–47], the energy shift associated with going from a point nucleus to a nucleus of finite size is expressed in terms of perturbation theory and evaluated separately for the ground and excited nuclear state. This is hardly a viable approach in a relativistic framework due to the weak singularity of the electron density at the nucleus. We therefore follow the approach of Filatov [19, 22] in which the isomer shift is calculated as an energy derivative. We start with the clamped-nucleus approximation in which a nucleus provides an electrostatic potential that depends on the nuclear charge density ρ_n as

$$\phi_n(\boldsymbol{r_e};R) = \int \mathrm{d}^3 r_n \, \frac{\rho_n(\boldsymbol{r_n};R)}{r_{ne}}, \tag{2}$$

where R is some model-specific radial size parameter that characterizes the extension of ρ_n [11, 13, 48]. The electrostatic electron–nucleus interaction is given by

$$E^{el}(R) = \int \rho_e(\boldsymbol{r_e})\phi_n(\boldsymbol{r_e};R)\mathrm{d}^3 r_e, \tag{3}$$

and is a function of the nuclear radius R. Following Filatov [19, 22], we calculate the associated shift in frequency of the emitted or absorbed photon as an energy derivative

$$\begin{aligned}\Delta E_\gamma &= \left.\frac{\partial E^{el}}{\partial R}\right|_{R=R_0} \Delta R \\ &= \left[\int \rho_e(\boldsymbol{r_e})\frac{\partial \phi_n(\boldsymbol{r_e})}{\partial R}\mathrm{d}^3 r_e + \int \frac{\partial \rho_e(\boldsymbol{r_e})}{\partial R}\phi_n(\boldsymbol{r_e})\mathrm{d}^3 r_e\right]_{R=R_0} \Delta R\end{aligned} \tag{4}$$

in which R_0 is the nuclear ground state radius and $\Delta R = R^\star - R_0$ the change in radius upon excitation, assumed to be much smaller than R_0. The first of the approximations made to derive the contact density expression is to assume that only the first term of Eq. 4 is relevant for the calculation of energy differences between emitting and absorbing nuclei, that is the change of electron density due to the nuclear excitation is not important in the calculation of the shift. This approximation is discussed by Fricke and Waber [49] who estimated the effect of the other term to be of the order of 0.2 to 0.4% of the isomer shift. We can thus take the difference derivative of the nuclear potential with respect to nuclear radius as a perturbing operator and calculate the energy differences for nuclei in chemically different environments via first-order perturbation theory.

The next step is to take a specific model for the charge density of the nucleus and establish an explicit expression for ΔE_γ. A detailed comparison of various models is given by Andrae [11, 13], and we refer to this work for illustrative plots of the various nuclear potentials. Relevant for the present discussion are the Gaussian model that is used to obtain relativistic electron densities, and the homogeneously charged sphere model. The potential of the latter one is

$$\phi_n^H(\boldsymbol{r}) = \begin{cases} \frac{Z}{2R}\left(3 - \frac{r^2}{R^2}\right); & r \le R \\ \frac{Z}{r}; & r > R \end{cases} \tag{5}$$

The corresponding derivative is

$$\frac{\partial \phi_n^H(\boldsymbol{r})}{\partial R} = \begin{cases} -\frac{3Z}{2R^2}\left(1 - \frac{r^2}{R^2}\right); & r \le R \\ 0; & r > R \end{cases} \tag{6}$$

If we assume that the variation of the electron density inside the nuclear volume is minimal, we may replace the function $\rho_e(\boldsymbol{r_e})$ in Eq. 4 by a constant effective density $\bar{\rho}_e$. We can then integrate over the nuclear volume to obtain a simple expression for the energy difference

$$\Delta E_\gamma = -\frac{4\pi}{5} Z \bar{\rho}_e R_0 \Delta R \tag{7}$$

In the Gaussian model, the nuclear charge distribution is given as

$$\rho_n^G(\boldsymbol{r}) = \rho_0 \exp\left[-r^2/R_G^2\right]; \quad \rho_0 = \frac{Z}{\left(\pi^{1/2} R_G\right)^3} \tag{8}$$

and the corresponding nuclear potential is expressed in terms of the error function

$$\phi_n^G(\boldsymbol{r}) = \frac{Z}{r}\mathrm{erf}(r/R_G). \tag{9}$$

The nuclear radius parameter R_G can be related to the radius parameter R of the homogeneous sphere model by comparing radial second momenta [11, 13]

$$\langle r^2\rangle = \frac{3}{2}R_G^2 = \frac{3}{5}R^2; \quad \Rightarrow \quad R_G = \sqrt{\frac{2}{5}}R \tag{10}$$

Taking the derivative with respect to the nuclear radius parameter R_G, we obtain a particularly simple expression

$$\frac{\partial\phi_n^G(\boldsymbol{r})}{\partial R} = -2\pi R_G\left(\frac{\partial R_G}{\partial R}\right)\rho_n^G = -\frac{4\pi}{5}R\rho_n^G \tag{11}$$

which, following the same procedure as for the homogeneous sphere, leads to an identical expression for the energy shift, that is Eq. 7. This relation can therefore also be used to retrieve the effective density by varying the radius parameter of the Gaussian model.

The effective density $\bar{\rho}_e$ is often approximated by the contact density, $\rho_e(0)$. The full sequence of approximations then reads

$$\begin{aligned}\Delta E_\gamma &\approx \left.\frac{\partial E^{el}}{\partial R}\right|_{R=R_0}\Delta R &&\approx \left[\int\rho_e(\boldsymbol{r_e})\frac{\partial\phi_n(\boldsymbol{r_e})}{\partial R}\mathrm{d}^3r_e\right]_{R=R_0}\Delta R\\ &\approx \left[\bar{\rho}_e\int\frac{\partial\phi_n(\boldsymbol{r_e})}{\partial R}\mathrm{d}^3r_e\right]_{R=R_0}\Delta R &&\approx \rho_e(0)\left[\int\frac{\partial\phi_n(\boldsymbol{r_e})}{\partial R}\mathrm{d}^3r_e\right]_{R=R_0}\Delta R\end{aligned} \tag{12}$$

As pointed out by Fricke and Waber [49], in the relativistic case, the last approximation is likely to be the most severe one and should in principle lead to an overestimation of energy differences as ρ_e (0) represents a maximum of the charge density. Assuming the intermediate approximations to be minor, we can assess the effect of this approximation by extracting the effective density $\bar{\rho}_e$ from the derivative of the energy with respect to nuclear radius and then compare with the calculated contact density ρ_e (0). Results of this procedure for the Gaussian model will be reported in Sect. 4.2

2.2 The contact density for two- and four-component wave functions

Since the electron density is an observable, an operator can be assigned to it, which yields the particle distribution at the point $\boldsymbol{r} = (x, y, z)$ in space. By multiplying the electron density with the negative elementary charge, one obtains the charge density $\rho_e(\boldsymbol{r}) = -en(\boldsymbol{r})$. The density operator $\hat{\rho}_{\boldsymbol{r}}$ then reads as

$$\hat{\rho}_{\boldsymbol{r}} = -e\sum_{i=1}^{N}\delta^{(3)}(\boldsymbol{r}-\boldsymbol{r}_i) \tag{13}$$

with $\delta^{(3)}(\boldsymbol{r}-\boldsymbol{r}_i)$ being the three-dimensional Dirac delta distribution. The density operator allows one to express the electron density as an expectation value. The electronic charge density for a four-component wave function described by a single Slater determinant is accordingly given by

$$\begin{aligned}\rho_e^{4c}(\boldsymbol{r}) &= \left\langle\Psi^{4c}(\{\boldsymbol{r}_i\})\middle|\hat{\rho}_{\boldsymbol{r}}\middle|\Psi^{4c}(\{\boldsymbol{r}_i\})\right\rangle\\ &= -e\sum_i^N\Psi_i^{4c\dagger}(\boldsymbol{r})\cdot\Psi_i^{4c}(\boldsymbol{r}),\end{aligned} \tag{14}$$

with Ψ_i^{4c} denoting a four-component orbital.

At the two-component relativistic level, the situation is much more complicated. The relevant Hamiltonian is obtained by carrying out an exact or approximate block diagonalization U of the parent four-component Dirac Hamiltonian H^{4c} and then retaining the block describing the positive energy spectrum only, that is, the two-component Hamiltonian is given by

$$H^{2c} = \left[U^\dagger H^{4c}U\right]_{++}. \tag{15}$$

Four-component property operators Ω^{4c} must be subject to the same decoupling transformation as the Hamiltonian, that is

$$\Omega^{2c} = \left[U^\dagger\Omega^{4c}U\right]_{++}. \tag{16}$$

Use of the approximate expression $\Omega^{2c} \approx \left[\Omega^{4c}\right]_{LL}$ leads to picture change errors (PCE) [50–52] that may be larger than the relativistic effects [53]. This observation also holds true for the density operator, which implies that at the two-component level the electron density cannot simply be resolved into a sum of the squared absolute values of the orbitals at the position $\boldsymbol{r}$ [17, 54–56], that is,

$$\rho^{2c}(\boldsymbol{r}) \neq -e\sum_i^N\Psi_i^{2c\dagger}(\boldsymbol{r})\cdot\Psi_i^{2c}(\boldsymbol{r}). \tag{17}$$

2.3 Projection analysis

For Hartree–Fock and DFT, it is natural to decompose the total electron density in terms of partial densities from the occupied molecular orbitals. Both the contact density and the averaged density defined in Sect. 2.1 are extremely local quantities and thus well-suited for analysis by means of the projection analysis introduced in Ref. [57]. In this method, the (occupied) molecular orbitals are expanded in pre-calculated orbitals of the constituent atoms

$$|\Psi_i\rangle = \sum_{Aj}|\Psi_j^A\rangle c_{ji}^A + |\Psi_i^{\mathrm{pol}}\rangle, \tag{18}$$

where the index A labels the individual atoms. In order to avoid overcompleteness and to obtain a meaningful analysis, the expansion is limited to the ground state-occupied orbitals

and possibly some virtual orbitals of each center. Whatever part of the molecular orbital $|\Psi_i\rangle$ which is not spanned by the reference orbitals is denoted the polarization contribution $|\Psi_i^{\mathrm{pol}}\rangle$ and is by construction orthogonal to those. Inserting the expansion into the SCF expectation value expression for a general operator $\hat{\Omega}$ leads to a series of terms

$$\langle\Psi|\hat{\Omega}|\Psi\rangle = \underbrace{\sum_A \sum_{ijk} \langle\Psi_i^A|\hat{\Omega}|\Psi_j^A\rangle c_{ik}^{A\star} c_{jk}^A}_{\text{intra-atomic}} + \underbrace{\sum_{A\neq B} \sum_{ijk} \langle\Psi_i^A|\hat{\Omega}|\Psi_j^B\rangle c_{ik}^{A\star} c_{jk}^B}_{\text{interatomic}} + (\text{pol}), \tag{19}$$

which can be conveniently divided into three classes: (1) the *intra-atomic contribution* involves only orbitals from a single center. It can be further subdivided into the principal moments involving only diagonal atomic matrix elements $\langle\Psi_i^A|\hat{\Omega}|\Psi_j^A\rangle$, (i = j) and hybridization contributions for which $i \neq j$. The principal moments contribute to the atomic expectation value, whereas the hybridization contribution arises from mixing of atomic orbitals in the molecular field (2) The *interatomic contribution* involves two centers, whereas (3) the *polarization contribution* involves the parts of the molecular orbitals not spanned by the selected atomic orbitals. The usefulness of the analysis is generally reduced if the polarization contribution is important, a feature that can be remedied by including more reference orbitals. However, in a comparative study as the present one, the polarization contribution does carry information, as will be seen in Sect. 4.4. Selecting $\hat{\Omega} = 1$ allows the formulation of a population analysis similar to the Mulliken one, but without the undesirable strong basis set dependence of the latter [58].

In the present study, we investigate the mercury contact density in various molecular species and calculate the shift $\Delta n(0)$ in the contact density with respect to the free atom. We may anticipate that the total expectation value will be dominated by intra-atomic contributions from the same center. Fixing our coordinate system at the mercury center, we write this contribution as

$$\Delta n_{\mathrm{Hg}}^{intra} = \sum_{pq} \left\langle \Psi_p^{\mathrm{Hg}\dagger} \middle| \delta^{(3)}(\boldsymbol{r}) \middle| \Psi_q^{\mathrm{Hg}} \right\rangle \Delta D_{pq}^{intra} \tag{20}$$

where the difference between the intra-atomic block of the density matrix of the molecular species under study and the isolated atom is given by

$$\Delta D_{pq}^{intra} = D_{pq}^{molecule;intra} - D_{pq}^{\mathrm{Hg};intra}; \quad D_{pq}^{intra} = \sum_i c_{pi}^{\mathrm{Hg}\star} c_{qi}^{\mathrm{Hg}}. \tag{21}$$

This expression can be analyzed further by inserting the explicit form of four-component relativistic atomic orbitals

$$\Psi = \begin{bmatrix} R^L(r)\chi_{\kappa,m_j}(\theta,\phi) \\ iR^S(r)\chi_{-\kappa,m_j}(\theta,\phi) \end{bmatrix} \tag{22}$$

where χ_{κ,m_j} are two-component angular functions.

The atomic matrix elements in Eq. 20 can now be expressed as

$$\left\langle \Psi_p^{\mathrm{Hg}\dagger} \middle| \delta^{(3)}(\boldsymbol{r}) \middle| \Psi_q^{\mathrm{Hg}} \right\rangle = \left\{ \left\langle R_p^L \middle| \frac{\delta(r)}{4\pi r^2} \middle| R_q^L \right\rangle_r \left\langle \chi_{\kappa_p,m_p} \middle| \chi_{\kappa_q,m_q} \right\rangle_{(\theta,\phi)} + \left\langle R_p^S \middle| \frac{\delta(r)}{4\pi r^2} \middle| R_q^S \right\rangle_r \left\langle \chi_{-\kappa_p,m_p} \middle| \chi_{-\kappa_q,m_q} \right\rangle_{(\theta,\phi)} \right\} \tag{23}$$

where subscripts r and (θ, ϕ) refer to radial and angular integration, respectively. From the angular integration, we find that non-zero contributions require that $\kappa_p = \kappa_q$ and $m_p = m_q$. The intra-atomic contribution to the relative contact density can therefore be written

$$\Delta n_{\mathrm{Hg}}^{intra} = \frac{1}{4\pi} \sum_{\substack{pq \\ \kappa_p=\kappa_q, m_p=m_q}} \left[R_p^L(0) R_q^L(0) + R_p^S(0) R_q^S(0) \right] \Delta D_{pq}^{intra} \tag{24}$$

To proceed, we now consider small r solutions of the Dirac equation for hydrogenic atoms [14, 15, 59]. We expand the large- and small-component radial functions as

$$\begin{aligned} R^L &= r^{\gamma-1}(p_0 + p_1 r + p_2 r^2 \ldots) \\ R^S &= r^{\gamma-1}(q_0 + q_1 r + q_2 r^2 \ldots) \end{aligned} \tag{25}$$

For a point nucleus $\gamma = \sqrt{\kappa^2 - Z^2/c^2} > |\kappa|$ such that there is a weak singularity for $|\kappa| = 1$. For an extended nucleus, as employed in this work, we have $\gamma = |\kappa|$. For $\kappa < 0$, we have $q_0 = p_1 = 0$, which implies that for $s_{1/2}$ orbitals $R^L(0) = p_0$ and $R^S(0) = 0$, where p_0 is determined from normalization. For $\kappa > 0$, we have $p_0 = q_1 = 0$, which implies that for $p_{1/2}$ orbitals $R^L(0) = 0$ and $R^S(0) = q_0$, where q_0 is likewise determined from normalization. This result can be compared to the non-relativistic case where the radial function is expanded as

$$R(r) = r^l(a_0 + a_1 r + a_2 r^2 + \cdots) \tag{26}$$

for both a point and extended nucleus (a_1 is zero for an extended nucleus, thus removing the cusp). In the non-relativistic case, we accordingly see that only s-orbitals have non-zero values at the nucleus, whereas in the relativistic case both $s_{1/2}$ and $p_{1/2}$ orbitals are non-zero at the origin.

3 Computational details

3.1 Effective densities

In order to assess errors induced by the replacement of the effective density $\bar{\rho}_e$ by the contact density $\rho_e(0)$, as in

Eq. 12, we have calculated the derivative of the energy with respect to the nuclear radius, using a Gaussian model for the nuclear charge distribution. This derivative was formulated as the derivative of the energy with respect to the radial *rms* value

$$\bar{\rho}_e = -\left[\frac{3}{4\pi Z\langle r^2\rangle^{1/2}}\frac{\partial E^{el}}{\partial\langle r^2\rangle^{1/2}}\right]_{R=R_0} \tag{27}$$

and was calculated numerically by taking step sizes significantly larger than the physical change in nuclear radius in the Mössbauer transition to avoid numerical inaccuracies. By checking linearity of the results, we found that a five-point finite difference scheme

$$\left.\frac{\partial E^{el}}{\partial\langle r^2\rangle^{1/2}}\right|_{R=R_0} = \frac{E(-2h) - 8E(-h) + 8E(+h) - E(+2h)}{12h}, \tag{28}$$

with a step size of $h = 5\cdot 10^{-7}a_0$ is sufficient to get numerically stable derivatives. Each energy value was calculated as an expectation value where the perturbation operator is the modification of the nuclear potential with respect to the default nuclear size. This allows us to decompose the effective density into contributions from individual molecular orbitals. As discussed in Sect. 2.3, only $s_{1/2}$- and $p_{1/2}$-type orbitals contribute to the contact density, through their large and small components, respectively. However, other orbitals may contribute to the effective density, as will be shown in Sect. 4.2

3.2 Electron correlation methods

Due to the dominant influence of the nuclear potential, the absolute magnitude of the density close to the Hg nucleus is already well described at the Hartree–Fock level. The isomer shift does, however, depend on the changes of density due to the chemical environment and is thus much more sensitive to the valence contributions. An accurate description of the valence electronic structure, which yields the most sensitive contributions to the contact density, requires to properly account for electron–electron correlation [23]. For this purpose, we performed Møller–Plesset second-order perturbation theory (MP2) as well as coupled-cluster (CC) calculations with a full iterative treatment of single and double excitations (CCSD) and including perturbative corrections for triple excitations (CCSD(T)) [60, 61]. Since all atomic and molecular compounds considered in the present study exhibit a closed-shell ground state (except for the monoradical HgF), the use of a single-determinant reference *ansatz* seems thus well justified. This belief is further corroborated by the T_1 diagnostics [62] which indicates the importance of single excitations in the CCSD approximation. For all closed-shell systems, the T_1 diagnostics was less than 0.023. The molecular radical HgF, on the other hand, has a $^2\Sigma^+_{\frac{1}{2}}$ ground state which in general calls for a multi-reference treatment. We therefore applied both the Fock-space coupled-cluster singles and doubles [63] (FS-CCSD) method, a genuine multi-reference CC method, and an open-shell CCSD(T) *ansatz* for the calculation of the ground state contact density. As the relative deviations in the electron densities between the two approaches was less than 10 ppm, we will in the following only refer to the open-shell CCSD(T) data.

An efficient and sophisticated approach to an analytic evaluation of the contact density at the CC level calls for, e.g., a general-order response theory framework [64] which is at present not available in our CC implementation. We have therefore chosen to rather pursue a finite-field strategy which has proven successful in the calculation for various valence and core properties, see e.g., Refs. [65–67]. In this approach, the contact density at a given nucleus is modeled by adding the density operator $\hat{\rho}_{\boldsymbol{r}}$ multiplied with a varying perturbation strength λ ("field strength") to the unperturbed Hamiltonian $\hat{H}^0$:

$$\hat{H}^0 + \hat{H}' = \hat{H}^0 + \lambda\cdot\hat{\rho}_{\boldsymbol{r}}. \tag{29}$$

The total electronic energy E becomes a function of the field strength λ, which allows to obtain the expectation value of the contact density from the first derivative of E(λ) with respect to λ

$$\rho(0) = \left.\frac{dE(\lambda)}{d\lambda}\right|_{\lambda=0}. \tag{30}$$

Comprehensive test studies on the Hg atom revealed an optimal field strength of $\lambda^{opt} = 10^{-8}$ which not only avoided contamination from higher-order contributions but also ensured numerically stable results independent from the level of relativity included in the Hamiltonian. Moreover, it turned out to be particularly useful to treat HF and correlation contributions to the total contact density separately, similar to the procedure followed in finite-field nuclear quadrupole moment calculations [68]. In so doing, we add to the HF expectation value of $\rho(0)$ (Eq. 13) the expectation value $\rho^{corr}(0)$ obtained from a numerical differentiation of the MP2/CCSD/CCSD(T) electron correlation energy E_{corr}

$$\rho^{total}(0) = \rho^{HF}(0) + \rho^{corr}(0) \tag{31}$$

It proved further advantageous that E_{corr} showed a nearly linear dependence on the perturbation strength λ which allowed us to use for the numerical differentiation the well-known central-difference method [69]. Sufficiently high accuracy could then already be achieved with a seven-point stencil

$$\rho^{corr}(0) = \frac{-E^{-3}_{corr} + 9E^{-2}_{corr} - 45E^{-1}_{corr} + 45E^{+1}_{corr} - 9E^{+2}_{corr} + E^{+3}_{corr}}{60\lambda^{opt}}, \tag{32}$$

where E^{n}_{corr} denotes the electron correlation energy calculated at a perturbation of $n \cdot \lambda^{opt}$.

We also carried out four-component density functional theory (DFT) calculations based on the Dirac–Coulomb (DC) Hamiltonian DFT calculations in order to investigate their performance in the evaluation of contact densities in comparison with wave function methods (WFM) such as HF and CC. For this purpose, an ample set of exchange-correlation functionals has been used, namely LDA (VWN5) [70, 71], BP86 [72, 73], BLYP [72, 74, 75], B3LYP [72, 76, 77], CAMB3LYP [78], PBE [79], and PBE0 [80]. Moreover, it will allow for a detailed examination of internal consistency within the DFT contact densities owing to the approximate nature of the functionals.

As pointed out by Neese [24], the numerical integration scheme must be carefully calibrated to reproduce the electron density in the core region. We therefore employed an ultrafine grid (using the `.ULTRAFINE` option in DIRAC) in order to ensure converged results in the exchange-correlation evaluation. The option implies the use of the basis-dependent radial integration scheme of Lindh et al. [81] with a convergence threshold of 2×10^{-15} and a 2D Lebedev angular integration correct to angular momentum $L = 64$. The grid size given as (radial points, angular points) thus reads as (237, 54) and (163, 142) for the Hg and F atomic center, respectively, when using the extended triple-ζ basis sets (see Sect. 3.4). The convergence of the contact density evaluation with respect to the grid size was validated by means of single-point calculations reverting to the standard grid definition in DIRAC which yielded identical results within numerical accuracy.

3.3 Hamiltonian operator

As outlined in the previous section, the scope of the study is twofold: besides the assessment of various electron correlation approaches, we also address successive approximations to the four-component DC Hamiltonian and the influence of spin-orbit coupling (SOC) in the evaluation of the contact density. In particular, we compare four-component relativistic results to:

- relativistic densities using the eXact two-Component (X2C) Hamiltonian [82];
- four-component spin-orbit free [83, 84] (scalar-relativistic) densities;
- one-component scalar-relativistic densities employing the Douglas–Kroll–Hess (DKH) Hamiltonian [85–91];
- non-relativistic densities employing the Lévy-Leblond [92] Hamiltonian.

The eXact two-Component (X2C) calculations have been carried out including two-electron spin-same-orbit corrections provided by the AMFI [93, 94] code. The four-component spin-orbit free (sfDC) as well as the Lévy-Leblond Hamiltonian are defined by a genuine parametrization of the DC Hamiltonian utilizing a quaternion modified Dirac equation [95]. In particular, no perturbation parameters are required for the separation into non-relativistic, scalar-relativistic and spin-dependent terms, respectively, and the Hamiltonians are thus in this sense exact. All these Hamiltonian schemes including the four-component DC Hamiltonian are available in the DIRAC10 program package [96], while the DKH Hamiltonians and properties are implemented in the MOLCAS 7.3 software suite [97]. For the latter calculations, we employ the notation DKH (n, m) [17] where n and m refer to the order of DKH transformation in the wave function and density operator, respectively, that is

$$\begin{aligned}\rho^{\mathrm{DKH(n,m)}}(\boldsymbol{r}) &= \left\langle \boldsymbol{U}^{(n)}\Psi(\{\boldsymbol{r}_i\}) \middle| \boldsymbol{U}^{(m)}\hat{\rho}_{\boldsymbol{r}}\boldsymbol{U}^{(m)\dagger} \middle| \boldsymbol{U}^{(n)}\Psi(\{\boldsymbol{r}\}) \right\rangle \\ &= -e\left\langle \Psi^{\mathrm{DKH},n}(\{\boldsymbol{r}_i\}) \middle| \sum_{k=1}^{m} \delta_{\epsilon,k}(\boldsymbol{r}) \middle| \Psi^{\mathrm{DKH},n}(\{\boldsymbol{r}_i\}) \right\rangle.\end{aligned} \tag{33}$$

For reasons of computational efficiency, the molecular mean-field approximation [98] to the four-component DC Hamiltonian was applied in all molecular wave-function-based calculations. In this scheme, the required set of two-electron integrals for the post-HF correlation step are computed in molecular orbital basis by neglecting all integrals of the AO basis that involve the small component. Nonetheless, the approximate integrals are combined with the exact orbital energies available from the HF solutions. The resulting Hamiltonian is denoted ^{4}DC** in Ref. [98]. The relative deviation in the total contact density from the exact ^{4}DC-CCSD(T), with the full set of two-electron integrals, was in all cases tested less than 0.1 ppm, and we therefore consider this as a reliable approach. For the purpose of investigating a potential importance of spin-other-orbit contributions for the evaluation of relative contact densities and reaction energies, we additionally performed molecular mean-field calculations based on the Dirac-Coulomb-Gaunt Hamiltonian. The latter Hamiltonian takes particularly into account both the charge-charge (Coulomb term) and the current–current instantaneous interactions between the electrons in the chosen reference frame [99].

Furthermore, as already discussed above, we have used a finite size Gaussian nuclear model with exponents taken from the reference tables provided by Visscher and Dyall

[100]. This approach avoids all singularities of the wave function that arise in point nucleus two- and four-component calculations.

3.4 Basis set considerations

Owing to the nature of the contact density as a core property, all calculations were carried out using atom-centered basis sets in their fully uncontracted form. In the relativistic four- and two-component as well as spin-orbit free and non-relativistic case, large-component scalar, Gaussian type orbitals (GTO) were employed. The small-component basis functions, if appropriate, were then generated by the restricted kinetic balance condition [95]. In the calculations performed with DIRAC triple-ζ (TZ) and quadruple-ζ (QZ), basis sets of Dyall [101, 102] were used for Hg. The starting large component TZ (QZ) $30s24p15d10f$ ($34s30p19d12f$) SCF set was augmented by $1f4g1h$ ($1f7g4h1i$) diffuse functions. Both TZ and QZ basis sets thus contain the primitives recommended for valence dipole polarization and valence correlation as well as for core-valence correlation. As fluorine basis the augmented correlation-consistent valence triple-ζ aug-cc-pVTZ (ATZ) and quadruple-ζ aug-cc-pVQZ (AQZ), basis sets [103] were chosen. The basis for the F atom was being left in uncontracted form to allow for valence polarization of the electron density around the neighboring Hg nucleus. In the scalar-relativistic DKH calculations, both the triple-ζ basis set of Dyall (see results in Table 5 as well as in Table C of the supporting information) and additionally also all-electron atomic natural orbital (ANO) sets for Hg and F [104–106] (see results in Table D in the supporting information) were employed in a completely decontracted manner.

To particularly ensure basis set saturation at the Hg nucleus with respect to an accurate computation of the contact density may nevertheless require an augmentation with tight s and p functions [18]. Our calibration studies at the Hartree–Fock level by means of the numerical atomic GRASP code [107] revealed a sufficient convergence by supplementing the Dyall TZ (QZ) basis set in an even-tempered fashion with two more tight $\{\zeta = 864721150.0, 230133640.0\}$ ($\{\zeta = 864477130.0, 230139440.0\}$) s functions and one tight $\{\zeta = 130716620.0\}$ ($\{\zeta = 194566990.0\}$) p function (see Table A in the supporting information for more details). The final large-component basis thus comprises a $[32s25p15d11f4g1h]$ ($[36s31p19d13f7g4h1i]$) set for Hg (denoted as TZ+2s1p(QZ+2s1p) for the following). Similarly, the uncontracted ANO basis set was augmented with two tight $\{\zeta = 993262470.3, 227944396.6\}s$ functions and one tight $\{\zeta = 91654636.2\}p$ function yielding a $[27s23p16d12f4g2h]$ set of primitives (denoted as ANO+2s1p).

3.5 Choice of active space

In the wave-function-based correlation methods, we chose two active spaces for the Hg atom and the mercury fluoride compounds HgF_n ($n = 1, 2, 4$). The first ("[v]") space comprises the valence $5d6s$ shell of mercury and the F $2s2p$ valence electrons. The second ("[cv]") space is a superset of the [v] space where the core $5s4f5p$ shells of Hg are additionally considered for correlation. The size of the virtual space included in [v] and [cv] was identical and consistently adapted for either basis set combinations TZ + 2s1p (Hg) + ATZ (F) and QZ + 2s1p (Hg)+ AQZ (F), respectively. In both cases, the virtual space limit for the [v] and [cv] spaces was tailored to contain all recommended core- and valence correlation as well as valence dipole polarization functions. This corresponds for the TZ set to a threshold of 95 hartree, whereas for the QZ set the cutoff is fixed at 107 hartree. For the Hg atom only, a third active space ("[all]") is furthermore taken into account. Here, the correlation treatment spans the full space of occupied and virtual orbitals.

4 Results and discussion

4.1 Molecular structures and energetics

Table 1 compiles the geometries for the series of molecular mercury fluoride species HgF_n ($n = 1, 2, 4$) for which contact densities have been computed. The geometries for the linear HgF_2 and square-planar HgF_4 molecules were taken from Ref. [41]. In this combined experimental and theoretical work, Wang and co-workers optimized the Hg-F bond length at the CCSD(T) level of theory using a small-core effective core-potential (ECP) combined with an augmented valence-basis set for Hg and an aug-cc-pVQZ one-particle basis for fluorine. They obtained Hg-F distances of 1.914 Å and 1.885 Å, respectively, for the di- and tetrafluoride mercury compound. Their values are in excellent agreement with the most recent two-component spin-orbit (SO) DFT and SO-CASPT2 data by Kim and co-workers [108] who report internuclear Hg-F distances of 1.912 Å and 1.884 Å (SO-PBE0) (1.886 Å; SO-CASPT2) for the two species. Moreover, the structural Hg-F parameters used in this work for both complexes fall within the range of data of 1.91–1.94 Å [37, 39, 108–111] and 1.88–1.89 Å [39, 108, 109], respectively, which is known from literature. The case is, however, different for HgF. Depending on the Hamiltonian, method and quality of basis sets applied the theoretically derived equilibrium bond distances r_e in the monoradical HgF comprise a spread of as large as 2.00–2.17 Å [37, 108, 110, 111] (see also Table 1 for a

Table 1 Spectroscopic constants (r_e and ω_e) for the ground state of the radical $^{202}Hg^{19}F$ calculated at the four-component Fock-space CCSD level correlating 40 electrons (Hg 5*s*5*p*4*f*5*d*, F 2*s*2*p*)

Molecule	Method	Basis sets (Hg/F)		r_e (Hg-F) [Å]	ω_e [cm^{-1}]
HgF	4c-FS-CCSD	TZ + 2s1p	ATZ[a]	2.012	509.2[b]
HgF	4c-FS-CCSD	QZ + 2s1p	AQZ	2.007	513.5
HgF	CCSD(T)[c]	ECP	ATZ	2.028	480.6
HgF	SO-PBE0[c]	ECP	ATZ	2.036	457.2
HgF	SO-M06-L[c]	ECP	ATZ	2.085	422.8
HgF	NESC/B3LYP[d]	DZ[e]	ATZ	2.080	–
HgF	B3LYP[f]	ECP	AQZ	2.076	414.7
HgF	QCISD[f]	ECP	6-311G(2df,2dp)	2.019	493.2
HgF	MP2[g]	ECP	6-311+G*	2.045	444.4
HgF_2	CCSD(T)	ECP	AQZ	1.914	–
HgF_4	CCSD(T)	ECP	AQZ	1.885	–

The energy truncation threshold for active virtual spinors was set at 95 and 107 hartree, respectively. In addition, geometries taken from Ref. [41] are reported for the HgF_n ($n = 2, 4$) compounds at which the present contact density calculations have been performed

[a] ATZ = aug-cc-pVTZ; AQZ = aug-cc-pVQZ

[b] Experimental value [113]: 490.8 cm^{-1}

[c] Ref. [108]

[d] Ref. [110]

[e] A contracted Dyall DZ basis was used

[f] Ref. [37]

[g] Ref. [111]

selection of data). Since furthermore no experimental data for r_e is available, this encouraged us to optimize the Hg-F bond distance at the four-component FS-CCSD level, thus providing a new theoretical reference value. In these benchmark calculations, we used the [cv] correlation space combined with the extensive QZ + 2s1p basis for Hg and the fluorine AQZ basis set in order to minimize the basis set superposition error. A description of the ground state of the radical diatom HgF by means of the FS-CCSD method requires a closed-shell starting electronic structure. We took the monocation as a point of departure and proceeded from the ground state of the ionic compound to the (0*h*,1*p*) Fock-space sector, thus arriving at the ground state of HgF:

$$HgF^{+}(0h, 0p) \rightarrow HgF(0h, 1p) \tag{34}$$

The active (0*h*,1*p*) sector space comprised the Hg 6*s* shell only. Trial studies at the TZ + 2s1p/ATZ basis set level with enlarged active spaces for the (0*h*,1*p*) sector did not reveal any significance of in particular the Hg 6*p* shell in terms of bonding participation. Moreover, using the same basis set combination, we also estimated the importance of core-valence electron correlation for the equilibrium bond length r_e. Extending the valence [v] to the core-valence [cv] correlation space yielded a bond length increase of 0.004 Å. The relative shift of −0.005 Å for Δ(QZ-TZ) in r_e (see also Table 1) is of same order of magnitude but of opposite sign. Our best theoretical estimate for r_e is thus 2.007 Å using the extended QZ basis sets and the [cv] electron correlation space, and all contact density calculations reported herein for the monoradical were carried out at this internuclear Hg-F distance. Looking at Table 1, it becomes obvious that our FS-CCSD value is located at the lower end of all existing theoretical predictions for r_e. Given the extensive basis sets, high level of correlation and *a priori* inclusion of spin-orbit coupling this benchmark nevertheless ought to be deemed close to the not yet measured equilibrium bond distance of HgF.

As can be seen from Eq. 34, the FS-CC scheme also allows to compute the ionization potential (IP of HgF as a by-product of the geometry optimization. We calculated the IP at the FS-CCSD[cv] correlation level using either the TZ or QZ basis sets. Our data of 232.0 kcal mol^{-1} and 233.2 kcal mol^{-1}, respectively, are in very good agreement with the IP of 235.3 kcal mol^{-1} reported by Cremer and co-workers [110] who derived their value from scalar-relativistic DFT calculations.

We also consider the elimination reaction of difluoride from the tetrafluoride mercury compound in the gas phase.

$$HgF_4 \rightarrow HgF_2 + F_2 \tag{35}$$

Among the rich thermochemistry of the mercury fluoride compounds HgF_n ($n = 1, 2, 4$) reaction (Eq. 35) has received particular attention in earlier theoretical and lately also experimental works [37, 39–41, 108, 109]. The

active interest originated from its importance in answering the question whether or not mercury is a genuine transition metal. Experimental studies in rare-gas matrices at low temperatures [41] recently confirmed the existence of HgF_4 which among the series of group 12 tetrafluorides MF_n (M = Zn, Cd, Hg) exhibits an endothermic F_2 elimination [38–40, 109, 112] only. Table 2 summarizes in this context our results obtained from single-point energy calculations in a four-component framework at the above discussed reference geometries for HgF_4 and HgF_2. Calculations on F_2 were carried out at the experimentally determined internuclear distance of $r_e = 1.41193$ Å [113]. Table 2 furthermore compiles a selection of reaction energies taken from previous scalar-relativistic and spin-orbit studies on the thermodynamical stability of HgF_4. We provide estimations for zero-point vibrational energy corrections to our four-component data by means of scalar-relativistic calculations using the Gaussian09 program [114]. In these vibrational frequency calculations, a small-core effective core-potential (ECP) combined with an augmented valence-basis set for Hg and an aug-cc-pVTZ (aug-cc-pVQZ) basis [103] for F (see Ref. [109] for more details on the Hg ECP/basis set) was used.

Table 2 Reaction energies (in kJ mol^{-1}) for the elimination reaction $HgF_4 \rightarrow HgF_2 + F_2$ in the gas phase calculated at different levels of theory within a four-component framework

Method	Basis set	Reaction energy
MP2	TZ + 2s1p	+67 (*+73*)
CCSD	TZ + 2s1p	+ 1 (+ *7*)
CCSD(T)	TZ + 2s1p	+31 (*+37*)
CCSD(T)[a]	TZ + 2s1p	+31 (*+37*)
CCSD(T)/DCG	TZ + 2s1p	+29 (*+35*)
CCSD(T)/sfDC	TZ + 2s1p	+20 (*+26*)
B3LYP/sfDC	TZ + 2s1p	+41 (*+48*)
B3LYP	TZ + 2s1p	+52 (*+59*)
	QZ + 2s1p	+54 (*+61*)
B3LYP[a]	TZ + 2s1p	+54 (*+61*)
PBE0	TZ + 2s1p	+60 (*+67*)
	QZ + 2s1p	+62 (*+69*)
CAMB3LYP	TZ + 2s1p	+52 (*+59*)
	QZ + 2s1p	+52 (*+60*)
Previous work	–	+36.3[b], +35.5[c], +9.5[c]
		+27.4[d]
		+41.0[e], +24.3[e]

Values in *italics* do not contain zero-point vibrational energy corrections. Calculations at the four-component spin-orbit free level are indicated with the abbreviation sfDC. Values marked with the acronym DCG were obtained based on the Dirac-Coulomb-Gaunt Hamiltonian using a molecular mean-field approximation

[a] Calculated at their respective geometries optimized at the four-component DFT/B3LYP/TZ + 2s1p level: HgF_4: 1.905 Å; HgF_2: 1.928 Å; F_2: 1.397 Å

[b] Ref. [39]: B3LYP value

[c] Ref. [109]: B3LYP and CCSD(T) values

[d] Ref. [41]: CCSD(T) value

[e] Ref. [108]: SO-M06 and CCSD(T) values

In accordance with earlier predictions, we find the tetrafluoride compound of mercury to be thermodynamically stable with respect to a spontaneous elimination of F_2 in the gas phase at 0 Kelvin. Turning to Table 2, we find that our four-component DFT data suggest a thermodynamically stable HgF_4 on the order of 50–60 kJ mol^{-1} varying with the chosen density functional. Summarizing our DFT results the F_2 elimination reaction seems slightly less favorable by about 10–20 kJ mol^{-1} when compared with earlier scalar-relativistic and spin-orbit DFT predictions by Riedel et al. [39], Wang et al. [41] as well as Kim and co-workers [108]. The correlated WFMs results compiled in Table 2, on the other hand, clearly reveal that both post-HF methods, MP2 and CCSD, may not be suitable to claim predictive character concerning the thermochemistry of mercury fluoride compounds. Only the successive inclusion of pertubative triples (CCSD(T); third row in Table 2) in our four-component calculations yields a reaction energy of 31 kJ mol^{-1} which is in very good agreement with the scalar-relativistic CCSD(T) data of 27.4 and 24.3 kJ mol^{-1} reported by Riedel et al. [109] and Kim et al. [108], respectively.

In order to reveal a potential significance of spin-same-orbit and in particular spin-other-orbit (SOO) coupling with regard to our present thermo chemistry data, we performed additional single-point CCSD(T) calculations based on the spin-orbit free (sfDC) and molecular mean-field Dirac-Coulomb-Gaunt Hamiltonian (DCG). Regarding the CCSD(T)/DC reaction energy value of 31 kJ mol^{-1} as our reference point, it can be seen from Table 2 that a consideration of SOO contributions in the evaluation of the thermo stability of HgF_4 leads to a slight correction of the CCSD(T)/DC value by 2 kJ mol^{-1}. A complete neglect of spin-orbit coupling contributions, on the other hand, gives rise to an underestimation by about −11 kJ mol^{-1}.

We conclude this paragraph by noting that the calculated reaction energies do not show any significant geometry dependence within computational error bars, neither with DFT nor with CCSD(T) (see for example third and fourth row in Table 2). For the purpose of comparison, we thus optimized the geometries of each reaction compound at the four-component DFT/B3LYP using the augmented TZ + 2s1p/ATZ basis sets for Hg and F, respectively.

4.2 Justification of the use of contact densities

Before we start with the calibration and interpretation of contact densities, we investigate the differences between

Table 3 Atomic matrix elements (HF/QZ + 2s1p)

	Contact density	Effective density
1s1/2	1951311.50	−194467.78
2s1/2	294993.24	−29548.24
3s1/2	67814.71	−6798.36
4s1/2	17035.79	−1708.17
5s1/2	3265.26	−327.42
6s1/2	276.32	−27.71
2p1/2	21856.04	−2107.28
2p3/2	0	2 × 0.51
3p1/2	5638.93	−544.14
3p3/2	0	2 × 0.14
4p1/2	1398.44	−134.96
4p3/2	0	2 × 0.03
5p1/2	237.17	−22.89
5p3/2	0	2 × 0.01
Total	2363827.39	−235685.57

For the contact density, we give absolute values; for the effective density, we give the difference between the effective density and the contact density. All values are in atomic units a_0^{-3}

the effective densities evaluated via Eq. 27 and the values obtained by directly evaluating the contact density. Table 3 lists the various contributions to the Hg atom densities for HF/QZ + 2s1p calculations. The results confirm that only the $s_{1/2}$ and $p_{1/2}$ orbitals contribute to the contact density, while the effective density also has small contributions from the $p_{3/2}$ orbitals. These $p_{3/2}$ contributions to the effective density arise due the fact that these orbitals reach a significant value inside the nuclear volume. We also observe similar contributions from $d_{3/2}$ orbitals (not shown). For other types of orbitals, the contributions are significantly smaller and not discernible from numerical noise. More importantly, the $s_{1/2}$ and $p_{1/2}$ contributions to the contact density are significantly higher than for the effective density. Interestingly, though, the deviation is quite systematically 10%.

Mössbauer spectroscopy is not concerned with absolute energies, but rather with energy shifts caused by the different chemical environment. Table 4 lists the contact and effective density *shifts* of the mercury fluorides relative to the mercury atom for HF/QZ + 2s1p calculations. Also

Table 4 Contact and effective densities differences relative to the Hg atom (HF/QZ + 2s1p)

	Contact density	Effective density
HgF	−114.54	−103.05
HgF_2	−127.85	−115.01
HgF_4	−98.09	−88.22

All values are in atomic units a_0^{-3}

here, we see significant deviations, but systematically on the order of 10%. This feature suggests that a calibration approach similar to that of Neese [24, 25] can be employed, thus justifying the use of contact densities for the determination of Mössbauer isomer shifts for elements as heavy as mercury. However, we will demonstrate in the next section that a DFT scheme, such as proposed by Neese [24, 25], does not even qualitatively reproduce the trends observed in relative contact densities between the fluorides of mercury.

4.3 Calibration of contact densities

We have compiled in Table 5 the mercury contact densities calculated in this work using the TZ + 2s1p/ATZ basis set combination (corresponding QZ + 2s1p/AQZ values are listed in Table B in the supporting information). For the Hg atom, we give absolute values, whereas for the mercury fluorides HgF_n ($n = 1, 2, 4$), we give values relative to the Hg atom, which seems most pertinent with respect to Mössbauer spectroscopy. The first entry is the four-component relativistic Hartree–Fock value. It is compared to the HF values obtained with neglect of the (*SS*|*SS*) class of two-electron Coulomb integrals in building the Fock matrix. As this approximation is usually accompanied with a Simple Coulombic Correction (SCC) [115] to correct for errors made in energy evaluation, we denoted this approach as HF[scc] in the table. It can be seen that this leads to errors of around 0.1 % for the absolute and relative contact densities with respect to the reference HF value and shows that this is probably a viable approximation for the calculation of contact densities even for heavy elements. At the SCF level, the SCC gives significant computational savings and is certainly recommended for the calculation of spectroscopic constants. However, in the present work, we have chosen not to invoke the SCC since our focus was on calibration and since SCC does not yield computational savings at the correlated WFM level, that is, once the four-index transformation to molecular orbital basis has been carried out. We next observe that spin-orbit free HF calculations (the Hamiltonian denoted sfDC in the table) give an error on the order of one percent for the absolute contact density of the Hg atom, but larger errors (up to 5%) for the relative values for the molecules. Such errors may not be acceptable, and it is therefore judicious to include spin-orbit coupling variationally in the calculation of contact densities of heavy atoms. Adding spin-other orbit (SOO) interaction through the Gaunt term (entry DCG) has only a minor effect on absolute and relative contact densities and can be ignored for these systems. What is certainly clear is that the use of a non-relativistic Hamiltonian is meaningless (Lévy-Leblond Hamiltoninan: LL in the table), as it gives orders of magnitude errors for both absolute and,

Table 5 Calculated mercury contact densities

Method	Hamiltonian	Hg	HgF	HgF_2	HgF_4
HF	DC	2363929.12	−114.48	−127.92	−98.09
HF	DCG	2354927.26	−113.83	−127.16	−97.22
HF[scc]	DC	2366645.73	−114.51	−127.83	−97.65
HF	sfDC	2342622.43	−115.59	−130.69	−103.52
HF	LL	361818.93	−11.92	−13.35	−6.77
HF	X2C	2358245.44	−114.06	−127.40	−97.43
HF	X2C[pce]	7579179.34	−712.55	−432.86	−350.65
HF	DKH(10,8)	2359971.35	−107.65	−131.33	−103.81
CCSD(T)[all]	DC	2364016.40			
CCSD(T)[cv]	DC	2363990.74	−95.11	−110.46	−104.16
CCSD(T)[cv]	DCG	2354988.44	–	−109.70	−103.20
CCSD(T)[v]	DC	2363952.83	−95.35	−110.55	−101.54
CCSD[all]	DC	2364013.22			
CCSD[cv]	DC	2363988.25	−94.33	−116.59	−105.16
CCSD[cv]	DCG	2354985.97	–	−115.79	−104.18
CCSD[v]	DC	2363952.22	−94.39	−115.93	−102.18
MP2[all]	DC	2364050.05			
MP2[cv]	DC	2364020.01	−95.10	−121.99	−124.34
MP2[v]	DC	2363963.15	−96.78	−118.88	−115.16
LDA	DC	2362802.35	−74.38	−99.03	−113.69
LDA	DKH(10,8)	2359359.64	−74.33	−103.75	−120.77
BP86	DC	2373796.03	−74.35	−98.52	−114.00
BLYP	DC	2373687.69	−72.82	−95.88	−111.48
B3LYP	DC	2370863.15	−85.86	−105.87	−113.54
CAMB3LYP	DC	2371811.55	−95.79	−113.92	−116.38
PBE	DC	2372713.57	−75.11	−98.74	−113.42
PBE0	DC	2370507.83	−91.30	−111.07	−115.62

For the Hg atom, we give absolute values, and for the mercury fluorides HgF_n ($n = 1, 2, 4$), we give values relative to the atom. All values are in atomic units a_0^{-3}. The acronym DC(G) refers to the Dirac-Coulomb(-Gaunt) Hamiltonian and sfDC to its spin-orbit free form. LL is the non-relativistic four-component Levy-Leblond Hamiltonian. DKH(10,8) corresponds to the 10-th order scalar-relativistic DKH Hamiltonian and 8-th order density operator. For explanation of other notation, see text (all results for Dyall's decontracted TZ+2s1p)

most importantly, relative contact densities. We furthermore see no simple linear relation between relativistic and non-relativistic HF contact densities.

The exact two-Component relativistic Hamiltonian (X2C) [82] performs very well compared to the four-component Dirac Hamiltonian provided the density operator is correctly transformed. The use of the untransformed density operator (denoted XCE[pce] in the table) leads to catastrophic picture change errors. The absolute and relative contact densities as well as the values relative to the atomic density, obtained with the DKH(10,8) Hamiltonian, are somewhat larger than those obtained for the X2C Hamiltonian (which is equivalent to the infinite-order DKH Hamiltonian). Note that even orders of the property-operator transformation approach the infinite-order result from above, whereas odd orders approach it from below [18] (as can be seen in Table D of the supporting information). We also find that in the DKH calculations it is possible to reduce the total number of primitive basis functions by decontracting only the s- and p-shells instead of using fully decontracted basis sets. The deviation for the DKH(10,8) Hartree–Fock contact densities of the mercury species is smaller than 0.1%, when employing the partially decontracted ANO-RCC basis set instead of the fully decontracted one (see Table E of the supporting information).

We next turn to the study of correlation effects in the calculation of contact densities. Comparing our HF value for the Hg atom with the value obtained from CCSD(T) with all electrons correlated (denoted CCSD(T)[all] in the table), we find that the error is extremely small, on the order of 40 pm. While this value is probably not converged with respect to the one-particle basis, the use of uncontracted sets should give a reasonable estimate of the size of core correlation contributions. The small value is perhaps not entirely

surprising since we are considering a closed-shell system dominated by a single Slater determinant. However, these errors are on the order of the *relative* contact densities. The correlation errors for these quantities are therefore significant, as seen for the other wave-function-based correlation methods listed in Table 5. For instance, with respect to CCSD(T) calculations including core-valence correlation (denoted CCSD(T)[cv] in the table), HF gives errors around 15% for HgF and HgF_2, whereas an error of −5% is observed for HgF_4. This clearly shows that electron correlation is mandatory for the calculation of relative contact densities. The effect of core-valence correlation can be seen by comparing our CCSD(T)[cv] results with CCSD(T) values obtained obtained with valence correlation only (denoted CCSD(T)[v] in the table). For HgF and HgF_4, we observe errors on the order of a few percent, whereas the error is quite small for HgF_2. The effect of the inclusion of perturbative triples can be assessed by comparing CCSD(T)[cv] and CCSD[cv] values in the table. It can be seen that omitting the perturbative triples may lead to errors close to 6% (HgF_2). This calls for a study of the effect of the inclusion of iterative triple and higher excitations [116] on calculated relative contact densities. Such calculations are expensive but possible with the recent interfacing [117] of the MRCC code [118] of Kállay and co-workers with DIRAC. Comparing CCSD(T)[cv] and MP2[cv], we see errors in the relative values on the order of 10–20% which shows that MP2 cannot be recommended for the calculation of relative contact densities for these systems.

When considering the performance of DFT in the calculation of contact densities, two points should be taken into consideration: (1) Most of today's available approximate density functionals contain parameters that are fitted against experimental data such as atomization energies, electron affinities and reaction barrier heights (see for instance Ref. [119]). To our knowledge, contact densities and Mössbauer data do not enter such training data and so a good performance of semi-empirical density functionals is not guaranteed for these properties. (2) Relativistic DFT generally employs non-relativistic density functionals due to the limited availability of relativistic functionals [120–125]. However, computational studies [126–128] indicate that the effect of such relativistic corrections is negligible for spectroscopic constants. For core properties, here represented by the extreme case of the contact density, the situation is less clear. Turning now to Table 5, we find that all density functionals give errors on the order of 0.5% for the contact density of the mercury atom, with the exception of LDA for which the error is 0.05%, but still larger than the relative contact densities. Considering the performance of the different density functionals in the case of the scalar-relativistic DKH Hamiltonian, the same trends are observed as for the Dirac–Coulomb Hamiltonian, whereas the absolute values are smaller (see Table C in the supporting information). For the molecular shifts, the errors are significant, but less than observed with HF, with GGA functionals performing no better than LDA and hybrid functionals providing only a slight improvement.

4.4 Analysis of contact densities

In this section, we will investigate the contact density of the mercury atom in more detail using the projection analysis described in Sect. 2.3. Neese studied the composition of the contact density in terms of molecular orbitals [24]. We believe we can get more detailed information from a decomposition of this expectation value in terms of *atomic* orbitals. We have included the occupied orbitals of the constituent atoms in the analysis. For the mercury atom, we also considered the virtual 6*p* orbitals since their role in bonding has been discussed in the literature [111].

The electron configuration of the mercury atom in the studied molecules, obtained by projection analysis at the HF level, is given in Table 6. In mercury monofluoride, the singly occupied HOMO is dominated (74.2 %) by the Hg $6s_{1/2}$ orbital, with some contributions (8.5%) from the fluorine 2*p*-orbitals. The HOMO-1 orbital has some contributions from Hg 5*d* which are, however, suppressed upon Pipek–Mezey localization [58, 129] of the closed-shell occupied orbitals, giving an orbital dominated by F 2*p* (78.1%), 2*s* (7.1%) and Hg $6s_{1/2}$ (12.0%). We find only minor contributions from Hg 6*p*, contrary to the analysis of Schwerdtfeger et al. [111], and the bonding corresponds rather to the three-electron two-orbital model discussed by Cremer et al. [110]. These findings corroborate also our conclusions from the FS-CCSD calculations in Sect. 4.1 where the inclusion of the Hg 6*p* in the model space did not lead to any measurable alteration in the optimized equilibrium structure. In HgF_2 and HgF_4, we likewise observe a very limited contribution from the Hg 6*p* orbitals. Along the HgF_n (n = 1, 2, 4) series, we observe an increasingly positive charge on the mercury atom, reaching +2.47 for HgF_4, still far from a formal charge of +4 suggested by the oxidation state, indicating increasing covalent character of

Table 6 Electron configuration and charge Q of mercury (gross populations) in the studied molecules obtained by projection analysis at the HF level

	HgF	HgF_2	HgF_4
5d	9.93	9.74	8.98
6s	1.08	0.68	0.48
6p	0.11	0.07	0.07
Q	0.88	1.51	2.47

bonding in the series [112]. At the DFT level, the covalent contributions to bonding are further strengthened and the 6*p* contributions increase slightly, as seen from Table 7. We also note that mercury atomic charges are systematically smaller at the DFT level than at the HF level.

We now turn to a projection analysis of the contact density at the HF level. The results are collected in Table 8. We expect the fluorine ligands to pull density away from the mercury atom, and we indeed observe that the contact density is reduced for all the molecular species with respect to the ground state atom. However, referring now to Table 5, we conclude that the decrease is not monotonous with respect to the number of fluorine ligands. This is in contrast to what is observed with all DFT functionals employed in this work, as well as MP2[cv]. The trend, however, agrees with the results obtained at the MP2[v] and coupled-cluster level. Turning now back to Table 8, we see that the (relative) contact density is indeed a very local quantity. The interatomic contribution as well as the intra-atomic contribution from the fluorine(s) are negligible. The polarization contribution, on the other hand, grows steadily along the series HgF_n ($n = 1, 2, 4$), reaching -72% for HgF_4. This contribution can certainly not be ignored and we shall return to it in the following.

Table 7 Electron configuration and charge Q of mercury (gross populations) in the studied molecules obtained by projection analysis at the DFT level using the B3LYP(LDA) functional

	HgF	HgF_2	HgF_4
5d	9.91 (9.90)	9.71 (9.71)	9.18 (9.22)
6s	1.29 (1.36)	0.89 (0.97)	0.56 (0.61)
6p	0.17 (0.19)	0.15 (0.20)	0.20 (0.28)
Q	0.63 (0.55)	1.24 (1.12)	2.07 (1.89)

Table 8 Projection analysis of Hg contact density, relative to the ground state atom, at the HF level

	HgF	HgF_2	HgF_4
Intra-atomic contribution			
Hg	−120.33	−161.99	−168.41
pm	−117.32	−178.30	−185.46
core	10.05	23.85	49.14
$6s_{1/2}$	−127.37	−202.15	−234.60
$6p_{1/2}$	0.06	0.01	0.01
hybrid	−3.01	16.32	17.06
F	0.00	0.00	0.00
Interatomic contribution	−0.07	−0.33	−0.53
Polarization contribution	5.93	34.39	70.84
Total	−114.48	−127.92	−98.09

The entries 'pm' and 'hybrid' refer to principal moments and hybridization contributions, respectively. All numbers are in atomic units a_0^{-3}

The relative Hg contact density is indeed dominated by the intra-atomic contribution from mercury, as one could expect, and can therefore be rationalized in terms of changes in $s_{1/2}$ and $p_{1/2}$ populations from the free atom to the molecule, as discussed in Sect. 2.3. The non-zero diagonal atomic matrix elements over the density operator at the origin are given in Table 10. At the HF level, we observe an exponential decay $a\exp(-bn)$ of these elements with respect to the main quantum number n. For $s_{1/2}$ ($p_{1/2}$) orbitals the fitted parameters are $a = 1.08 \times 10^7 (4.78 \times 10^5)$ and $b = 1.69(1.50)$. We also note that for a given main quantum number n the ratio between a diagonal matrix element for the $s_{1/2}$ over the $p_{1/2}$ one is on the order of ten than rather than $1/c^2$, which one would naively expect. However, one should keep in mind that the pointwise ratio between large and small components goes rather like v/c than $1/c$. [130]. In Table 10 we also give the relative deviation with respect to HF of corresponding atomic matrix elements calculated with the various DFT functionals employed in this study. Interestingly, the relative deviations grow as one goes from core to valence orbitals. This suggests that the observed deviations are not to be attributed to a particular failure of the approximate DFT functionals in the description of the core orbitals.

Returning now to Table 8, we see that the intra-atomic Hg contribution is dominated by the principal moments, although the hybridization contribution grows in importance with an increasing number of fluorine ligands. For the principal moments, we find that the contribution from the $6p_{1/2}$ orbital is negligible for all systems, albeit non-zero, in accordance with the analysis in Sect. 2.3. The relative contact density for the three molecules is dominated by the contribution from the Hg $6s_{1/2}$ orbitals. For this contribution, we observe a monotonic decrease of the contact density relative to the atom which is directly related to the corresponding decrease in the $6s_{1/2}$ population shown in Table 6. We can therefore conclude that the non-monotonic trend observed for the total relative contact density at the HF and CC level is related to the increasing polarization of the mercury $s_{1/2}$ orbitals in the molecule, indicated by the growing importance of the hybridization and polarization contributions, as the number of fluorine ligands increase. Indeed, for HgF_4 we find that successively adding the mercury $7s_{1/2}$, $8s_{1/2}$ and $9s_{1/2}$ orbitals reduces the polarization contribution from 70.84 to 52.07, 10.98 and $-2.89\,a_0^{-3}$, respectively.

The corresponding projection analysis at the DFT level is given in Table 9, and the most important contributions at the HF and LDA level are contrasted in Fig. 1. Comparing first Tables 6 and 7, we see that the $6s_{1/2}$ population is

Table 9 Projection analysis of Hg contact density, relative to the ground state atom, at the DFT level using the B3LYP(LDA) functional

	HgF	HgF_2	HgF_4
Intra-atomic contribution			
Hg	−100.69 (−93.96)	−147.93 (−142.40)	−180.05 (−180.52)
pm	−100.40 (−94.22)	−171.60 (−168.58)	−195.90 (−200.33)
core	11.99 (11.74)	25.13 (23.59)	58.51 (56.32)
$6s_{1/2}$	−112.38 (−105.96)	−196.73 (−192.17)	−254.41 (−256.65)
$6p_{1/2}$	0.21 (0.29)	0.11 (0.20)	0.13 (0.25)
hybrid	−0.29 (0.26)	23.66 (26.18)	15.85 (19.81)
F	0.00	0.00	0.00
Interatomic contribution	−0.11 (−0.11)	−0.41 (−0.41)	−0.65 (−0.67)
Polarization contribution	14.93 (19.69)	42.46 (43.78)	67.17 (67.50)
Total	−85.86 (−74.38)	−105.88 (−99.03)	−113.54 (−113.69)

The entries 'pm' and 'hybrid' refer to principal moments and hybridization contributions, respectively. All numbers are in atomic units a_0^{-3}

systematically lower at the HF level than at the DFT level, thus leading to higher atomic charges with the former method. This is contrary to what one would expect from looking at the $6s_{1/2}$ orbital energy in the neutral atom, which at the TZ+2s1p level is $-0.328\,E_h$, $-0.261\,E_h$ and $-0.274\,E_h$ at the HF, LDA and B3LYP levels, respectively. DFT, however, yields a more compact $6s_{1/2}$ orbital (the radial *rms* value is $4.33\,a_0$, $4.06\,a_0$ and $4.14\,a_0$ for HF, LDA and B3LYP, respectively) which in turn leads to a smaller polarizability [131] and larger contact density (cf. Table 10). The larger contact density leads to a crossover between the $6s_{1/2}$ contributions from HF and DFT when going from HgF_2 and HgF_4, as seen in Fig. 1. We also note from Tables 6 and 7 that whereas the 5*d* populations are rather similar at the HF and DFT level for HgF and HgF_2, there is a more significant drop at the HF level when going to HgF_4. Due to larger effective mercury atomic charge at the HF level, one would expect stronger polarization of the $6s_{1/2}$ orbital at the HF than the DFT level. However, this will be counterbalanced by the more compact nature and thus lower polarizability of the $6s_{1/2}$ orbital at the DFT level, as well as that there is less $6s_{1/2}$ population to polarize at the HF level, due to lower occupation. In practice, we find that for both HgF and HgF_2 the combined LDA contribution of polarization and hybridization is about $18\,a_0^{-3}$ larger than for HF, whereas this difference basically vanishes for HgF_4. A similar picture emerges when comparing HF and B3LYP. In conclusion, we see that there is a delicate balance between polarization and electron withdrawal, which in the case of DFT leads to a monotonous decrease of contact density along the series HgF_n ($n = 1, 2, 4$), but not for HF, the latter in agreement with our benchmark CC results.

An interesting final point from Tables 8 and 9 is that the contribution from the core $s_{1/2}$-orbitals to the principal moments is positive. This seemingly counter-intuitive result is due to the small, but generally non-zero overlap between Hg core orbitals and fluorine atomic orbitals. One can easily show that diagonal elements corresponding to Hg core orbitals of the intra-atomic block of the density matrix appearing in Eq. 21 are

$$D_{pp}^{intra} = 1 + \varepsilon^2 + O(\varepsilon^4) \tag{36}$$

where ε is the norm of the overlap in question.

Table 10 Atomic matrix elements (HF/TZ + 2s1p)

	HF	LDA	BP86	BLYP	B3LYP	CAMB3LYP	PBE	PBE0
$1s_{1/2}$	1951309.48	−0.10	0.37	0.36	0.25	0.29	0.32	0.24
$2s_{1/2}$	294992.89	−0.05	0.44	0.43	0.30	0.35	0.38	0.29
$3s_{1/2}$	67814.67	−0.16	0.36	0.34	0.24	0.28	0.31	0.24
$4s_{1/2}$	17035.91	1.94	2.17	2.20	1.74	1.79	2.11	1.58
$5s_{1/2}$	3265.25	9.54	8.96	9.13	7.30	7.32	8.74	6.46
$6s_{1/2}$	276.31	17.34	16.41	14.69	12.84	13.15	15.89	13.45
$2p_{1/2}$	21934.06	1.03	1.53	1.52	1.18	1.23	1.45	1.08
$3p_{1/2}$	5659.07	0.89	1.38	1.38	1.06	1.11	1.30	0.97
$4p_{1/2}$	1403.46	2.88	3.04	3.09	2.45	2.51	2.96	2.20
$5p_{1/2}$	238.01	10.68	9.94	10.14	8.10	8.02	9.66	7.11

For HF, we give absolute values in atomic units; for DFT functionals, we give deviations with respect to HF in %

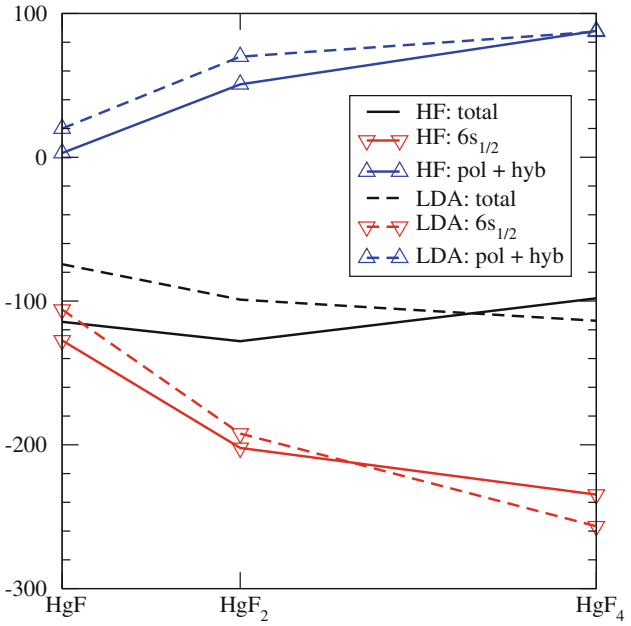

Fig. 1 Dominant contributions (in atomic units a_0^{-3}) to projection analysis of relative contact densities at the HF and LDA level. *pol* polarization, *hyb* hybridization

5 Conclusions and perspectives

The objective of this study has been to evaluate the performance of two- and four-component relativistic *ab initio* wave function methods and density functional theory approaches in the prediction of the Mössbauer isomer shift (IS) for compounds containing heavy elements using a contact density approach. In the recent past, various computational approaches [19, 23, 24] to the calculation of the IS in molecular systems containing lighter elements such as, e.g., ^{57}Fe, have been proposed and successfully applied. Entering the domain of heavy element chemistry, we therefore here focused on the series of mercury fluorides HgF_n ($n = 1, 2, 4$) where Hg exhibits two Mössbauer active isotopes, ^{199}Hg and ^{201}Hg.

The geometries for the di- and tetrafluoride compounds have been taken from a recently published scalar-relativistic study [41], whereas for the monoradical HgF we performed a geometry optimization at the relativistic four-component Fock-space CCSD level using augmented basis sets of quadruple-ζ quality. Based on our results, we propose new theoretical reference values for the internuclear distance r_e and harmonic frequency ω_e, that are 2.007 Å and 513.5 cm^{-1}, respectively. In addition, we find an excellent agreement with existing theoretical predictions concerning the ionization potential of HgF. Besides, on the basis of our benchmark, we could safely rule out a previously discussed distinct contribution of the Hg 6*p* shell to the bonding pattern in the monofluoride radical [111].

Gross population analysis along the HgF_n series reveals an increasing positive charge on the Hg central atom yielding a maximum of +2.47 in HgF_4 at the HF level. We attribute the significantly lower charge (the formal oxidation state of mercury is +IV) to a considerable proportion of covalent bonding in the square-planar tetrafluoride mercury complex. In addition, we estimate for the latter system the elimination reaction energy at the four-component coupled-cluster level regarding the decomposition of HgF_4 into HgF_2 and F_2 in gas phase. Our results computed at both literature reference geometries and herein at the four-component DFT level optimized structures are in excellent agreement with previous scalar-relativistic studies based on the use of effective core-potentials [108, 109]. It is shown that the neglect of spin-same-orbit contributions may lead to a severe underestimation of the elimination reaction energy whereas spin-other-orbit contributions are of minor importance.

Our calibration study shows that our selection of density functionals gives errors in the absolute contact density for the neutral mercury atom on the order of 0.5% compared to the CCSD(T) reference data. This is not only significantly larger than HF, but about two orders of magnitude larger than the relative density shifts observed in the molecular species with respect to the neutral atom. Contrary to what was found for ^{57}Fe Mössbauer IS by Neese [24], DFT is not able to qualitatively reproduce the non-monotonic decrease of the contact density of the heavier atom mercury that we obtain from our benchmark CCSD(T) calculations and even at the HF level. Projection analysis shows the expected monotonic decrease of the $6s_{1/2}$ contribution to the relative contact density with an increasing number of binding fluorine atoms, but this contribution is opposed by the increasing contributions of polarization and hybridization. For HgF_4, these latter contributions are quite similar at the HF and DFT level, but the more compact $6s_{1/2}$ orbital provided by DFT gives a larger contact density which in turn assures a monotonic decrease of the total value.

In order to further investigate the predictive value of approximate DFT functionals in the relativistic domain, it will thus be worthwhile to extent the present study to other heavy element containing systems such as ^{197}Au compounds for which a growing number of experimental Mössbauer IS data is available (see Refs. [132–136] and references therein). Aiming at a comprehensive assessment, one could furthermore take into account complexes of Mössbauer active isotopes such as ^{127}I or ^{129,131}Xe for which it would be interesting to study the $p_{1/2}$ contributions to the relative shift. Concerning the performance of the coupled-cluster wave function methods, on the other hand, we observe a partially distinctive effect of the inclusion of perturbative triples on the relative shift of the electron density. Although T_1 diagnostics at the CCSD level

indicate a justified use of a single-reference *ansatz*, we will look in more detail into the effect of including full triples as well as higher excitations on relative shifts of the electron density in a forthcoming publication thereby exploiting the recent interface [117] of the DIRAC10 program package [96] to a genuine and efficient multi-reference coupled-cluster code [118].

Finally, we have also assessed the application of the contact density approximation for calculating the Mössbauer IS which most notably assumes a constant electronic charge distribution over the finite-sized nucleus. Relying on a Gaussian model of the nuclear charge distribution, the contact density approach yields a systematic overestimation of 10% of the relative shifts along the HgF_n ($n = 1, 2, 4$) series when compared to the more sophisticated effective density approach (that is, the integration of the electron density over the nuclear volume). The systematic nature of the observed error, however, allows us to derive a correction factor which facilitates the calculation of Mössbauer ISs within the computationally straightforward contact density *ansatz*.

Acknowledgments We dedicate this paper to Pekka Pyykkö, a pioneer of relativistic quantum chemistry. With a unique combination of impressive chemical insight and judicious pragmatism, he has picked many of the bigger berries in the field, but graciously left some for others as well. We would like to thank one of the unknown referee's for her/his elaborate report and comments which led to the discovery of an initial computational problem in the calculation of reaction energies and contact densities of the HgF_4 compound. This issue has then been solved for the final version of this paper. S.K. thanks l'Université de Strasbourg (UDS) for a post-doctoral research grant and the supercomputer centers at ETH Zürich as well as UDS for ample computing time. M.R. and S.F. gratefully acknowledge financial support by ETH Zürich (Grant TH-26 07-3) and the Swiss national science foundation SNF (project no. 200020-132542/1). L.V. has been supported by NWO through the VICI programme.

References

1. Pyykkö P, Desclaux J-P (1979) Relativity and the periodic system of elements. Acc Chem Res 12(8):276–281
2. Pitzer KS (1979) Relativistic effects on chemical properties. Acc Chem Res 12(8):271–276
3. Pyykkö P (1988) Relativistic effects in structural chemistry. Chem Rev 88:563–594
4. Mössbauer RL (1958) Kernresonanzabsorption von Gammastrahlung in ^{191}Ir. Naturwissenschaften 45:538–539
5. Mössbauer RL (1958) Kernresonanzfluoreszenz von Gammastrahlung in ^{191}Ir. Z Phys 151:124–143
6. Greenwood NN, Gibb TC (eds) (1971) Mössbauer Spectroscopy. Chapman and Hall, London
7. Gibb TC (eds) (1976) Principles of Mössbauer spectroscopy. Chapman and Hall, London
8. Gütlich P, Link R, Trautwein A (eds) (1978) Mössbauer spectroscopy and transition metal chemistry. Springer, Berlin
9. Gütlich P, Schröder C (2010) Mössbauer spectroscopy. Bunsenmagazin 12:4–22
10. Kato T (1957) On the eigenfunctions of many-particle systems in quantum mechanics. Comm Pure Appl Math 10:151
11. Andrae D (2000) Finite nuclear charge density distributions in electronic structure calculations for atoms and molecules. Phys Rep 336:414–525
12. Andrae D, Reiher M, Hinze J (2000) A comparative study of finite nucleus models for low-lying states of few-electron high-Z atoms. Chem Phys Lett 320:457–468
13. Andrae D (2002) Nuclear charge density distributions in quantum chemistry. In: Schwerdtfeger P (ed) Relativistic electronic structure theory, part 1: fundamentals. Elsevier, Amsterdam
14. Dyall KG, Fægri K (2007) Introduction to relativistic quantum chemistry. Oxford University Press, Oxford
15. Quiney HM, Laerdahl JK, Faegri K, Saue T (1998) Ab initio Dirac-Hartree-Fock calculations of chemical properties and PT-odd effects in thallium fluoride. Phys Rev A 57:920
16. Andrae D, Reiher M, Hinze J (2000) Numerical electronic structure calculations for atoms. II. The generalized variable transformation in relativistic calculations. Int J Quantum Chem 76:473–499
17. Mastalerz R, Lindh R, Reiher M (2008) The Douglas–Kroll–Hess electron density at an atomic nucleus. Chem Phys Lett 465:157–164
18. Mastalerz R, Widmark P-O, Roos B-O, Lindh R, Reiher M (2010) Basis set representation of the electron density at an atomic nucleus. J Chem Phys 133:144111
19. Filatov M (2007) On the calculation of Mössbauer isomer shift. J Chem Phys 127:084101
20. Kurian R, Filatov M (2008) DFT approach to the calculation of Mössbauer isomer shifts. J Chem Theory Comput 4:278–285
21. Kurian R, Filatov M (2009) Calibration of ^{119}Sn isomer shift using ab initio wave function methods. J Chem Phys 130:124121
22. Filatov M (2009) First principles calculation of Mössbauer isomer shift. Coord Chem Rev 253:594–605
23. Kurian R, Filatov M (2010) Calibration of ^{57}Fe isomer shift from ab initio calculations: can theory and experiment reach an agreement? Phys Chem Chem Phys 12:2758–2762
24. Neese F (2002) Prediction and interpretation of the ^{57}Fe isomer shift in Mössbauer spectra by density functional theory. Inorg Chim Acta 337:181–192
25. Römelt M, Ye S, Neese F (2009) Calibration of modern density functional theory methods for the prediction of ^{57}Fe Mössbauer isomer shifts: meta-GGa and double-hybrid functionals. Inorg Chem 48:784–785
26. Carlson DE, Temperley AA (1969) Resonane absorption of the 32.2 keV gamma ray of ^{201}Hg. Phys Lett B 30:322–323
27. Walcher D (1971) Mössbaueruntersuchungen an ^{195}Pt und ^{201}Hg. Z Phys 246:123–150
28. Wurtinger W (1976) Mössbauer measurements on Hg-Pt-alloys using the 158 keV transition in ^{199}Hg. J Phys C 6:697–701
29. Koch W, Wagner FE, Flach D, Kalvius GM (1976) Mössbauer experiments with high energy gamma rays: the 158 keV transition in ^{199}Hg. J Phys C6:693–695
30. Wurtinger W, Kankeleit E (1979) ^{199}Hg Mössbauer measurements on mercury alloys and Hg-fluorides. Z Phys A 293:219–227
31. Lyle SJ, Westall WA (1984) A Mössbauer spectroscopic study of the Eu-Hg system. J Less-Common Met 99:265–272
32. Laubach S, Schwalbach P, Kankeleit E, Hasselbach K (1985) Electric hyperfine interaction in ^{199}Hg fluorides. Hyperfine Interact 23:259–271
33. Iranzo O, Thulstrup P, Ryu S-B, Hemmingsen L, Pecoraro V (2007) The application of ^{199}Hg NMR and ^{199m}Hg perturbed angular correlation (PAC) spectroscopy to define the biological

chemistry of Hg^{II}: a case study with designed two- and three-stranded coiled coils. Chem Eur J 13:9178–9190
34. Bieroń J, Pyykkö P, Jönsson P (2005) Nuclear quadrupole moment of ^{201}Hg. Phys Rev A 71:012502
35. Moon PB (1950) The hard components of scattered gamma-rays. Proc Phys Soc 63:1189
36. Malmfors KG (1953) Nuclear resonance scattering of gamma-rays. Arkiv för Fysik 6:49
37. Khalizov AF, Viswanathan B, Larregaray P, Ariya PA (2003) A theoretical study on the reactions of Hg with halogens: atmospheric implications. J Phys Chem A 107:6360–6365
38. Liu W, Franke R, Dolg M (1999) Relativistic ab initio and density functional theory calculations on the mercury fluorides: is HgF_4 thermodynamically stable? Chem Phys Lett 302:231–239
39. Riedel S, Straka M, Kaupp M (2004) Validation of density functional methods for computing structures and energies of mercury(IV) complexes. Phys Chem Chem Phys 6:1122–1127
40. Kaupp M, von Schnering HG (1993) Gaseous mercury(IV) fluoride, HgF_4: an ab initio study. Angew Chem Int Ed 32:861–863
41. Wang X, Andrews L, Riedel S, Kaupp M (2007) Mercury is a transition metal: the first experimental evidence for HgF_4. Angew Chem 119:8523–8527
42. Rooms JF, Wilson AV, Harvey I, Bridgeman AJ, Young NA (2008) Mercury-fluorine interactions: a matrix isolation investigation HgF_2, HgF_2 and HgF_4 in argon matrices. Phys Chem Chem Phys 10:4594–4605
43. Pyykkö P, Straka M, Patzschke M (2002) HgH_4 and HgH_6: further candidates for high-valent mercury compounds. Chem Comm 16:1728–1729
44. Shenoy GK, Wagner FE (1978) Mössbauer isomer shifts. North-Holland Publishing Company, Amsterdam
45. Rosenthal JE, Breit G (1932) The isotope shift in hyperfine structure. Phys Rev 41:459–470
46. Breit G (1958) Theory of isotope shift. Rev Mod Phys 30:507–516
47. Shirley DA (1964) Application and interpretation of isomer shifts. Rev Mod Phys 36:339–351
48. Bodmer AR (1953) Nuclear scattering of electrons and isotope shift. Proc Phys Soc A 66:1041–1058
49. Fricke B, Waber JT (1972) Calculation of isomer shift in Mössbauer spectroscopy. Phys Rev B 5:3445
50. Baerends EJ, Schwarz WHE, Schwerdtfeger P, Snijders JG (1990) Relativistic atomic orbital contractions and expansions—magnitudes and explanations. J Phys B: At Mol Opt Phys 23:3225–3240
51. Kellö V, Sadlej AJ (1998) Picture change and calculations of expectation values in approximative relativistic theories. Int J Quant Chem 68:159
52. Dyall KG (2000) Relativistic electric and magnetic property operators for two-component transformed hamiltonians. Int J Quant Chem 78:412
53. Pernpointer M, Schwerdtfeger P (1998) Accurate nuclear quadrupole moments of the gallium isotopes ^{69}Ga and ^{71}Ga within the PCNQM model. Chem Phys Lett 295:347
54. van Wüllen C, Michauk C (2005) Accurate and efficient treatment of two-electron contributions in quasirelativistic high-order Douglas-Kroll density-functional calculations. J Chem Phys 123:204113
55. Seino J, Uesugi W, Hada M (2010) Expectation values in two-component relativistic theories. J Chem Phys 132:164108
56. Bučinský L, Biskupič S, Jayatilaka D (2010) Picture change error correction of radon atom electron density. J Chem Phys 133:174125
57. Bast R, Koers A, Gomes ASP, Iliaš M, Visscher L, Schwerdtfeger P, Saue T (2010) Analysis of parity violation in chiral molecules. Phys Chem Chem Phys 13:854
58. Dubillard S, Rota J-B, Saue T, Fægri K (2007) Bonding analysis using localized relativistic orbitals: water, the ultrarelativistic case and the heavy homologues H2X (X = Te, Po, eka-Po). J Chem Phys 124:154307
59. Grant IP, Quiney HM (1988) Foundations of the relativistic theory of atomic and molecular structure. Adv At Mol Phys 23:37–86
60. Visscher L, Lee TJ, Dyall KG (1996) Formulation and implementation of a relativistic unrestricted coupled-cluster method including noniterative connected triples. J Chem Phys 105:8769
61. Pernpointner M, Visscher L (2003) Parallelization of four-component calculations. II. Symmetry-driven parallelization of the 4-Spinor CCSD algorithm. J Comp Chem 24:754
62. Lee TJ, Taylor PR (1989) A diagnostic for determining the quality of single-reference electron correlation methods. Int J Quantum Chem Symp 23:199
63. Visscher L, Eliav E, Kaldor U (2001) Formulation and implementation of the relativistic Fock-space coupled-cluster method for molecules. J Chem Phys 115:9720
64. Christiansen O, Jørgensen P, Hättig C (1998) Response functions from Fourier component variational perturbation theory applied to a time-averaged quasienergy. Int J Quantum Chem 68:1
65. Heßelmann A, Jansen G (1999) Molecular properties from coupled-cluster Brueckner orbitals. Chem Phys Lett 315:248–256
66. Knecht S, Sørensen LK, Jensen HJ Aa, Fleig T, Marian CM (2010) Accurate calculations of the ground state and low-lying excited states of the $(RbBa)^+$ molecular ion, a proposed system for ultracold reactive collisions. J Phys B: At Mol Opt Phys 43:055101
67. Jacob CR, Visscher L, Thierfelder C, Schwerdtfeger P (2007) Nuclear quadrupole moment of ^{139}La from relativistic electronic structure calculations of the electric field gradients in LaF, LaCl, LaBr, and LaI. J Chem Phys 127:204303
68. Pernpointner M, Visscher L (2001) Nuclear quadrupole moments for Al-27 and Ga-69 derived from four-component molecular coupled cluster calculations. J Chem Phys 114:10389
69. Hildebrand FB (1974) Introduction to numerical analysis. Dover Publications Inc, New York
70. Dirac PAM (1930) Note on exchange phenomena in the Thomas atom. Proc Roy Soc London 26:376
71. Vosko SH, Wilk L, Nusair M (1980) Accurate spin-dependent electron liquid correlation energies for local spin density calculations: a critical analysis. Can J Phys 58:1200–1211
72. Becke AD (1988) Density-functional exchange-energy approximation with correct asymptotic behavior. Phys Rev A 38:3098–3100
73. Perdew JP (1986) Density-functional approximation for the correlation energy of the inhomogeneous electron gas. Phys Rev B 33:8822–8824
74. Lee CT, Yang WT, Parr RG (1988) Development of the Colle–Salvetti correlation-energy formula into a functional of the electron-density. Phys Rev B 37:785–789
75. Miehlich B, Savin A, Stoll H, Preuss H (1989) Results obtained with the correlation-energy density functionals of Becke and Lee, Yang and Parr. Chem Phys Lett 157:200–206
76. Stephens PJ, Devlin FJ, Chabalowski CF, Frisch MJ (1994) Ab-initio calculation of vibrational absorption and circular-dichroism spectra using density-functional force-fields. J Phys Chem 98:11623–11627
77. Hertwig RH, Koch W (1997) On the parametrization of the local correlation functional: what is Becke-3-LYP? Chem Phys Lett 268:345–351
78. Yanai T, Tew DP, Handy NC (2004) A new hybrid exchange–correlation functional using the Coulomb-attenuating method (CAM-B3LYP). Chem Phys Lett 393:51–57

79. Perdew JP, Burke K, Ernzerhof M (1996) Generalized gradient approximation made simple. Phys Rev Lett 77:3865–3868
80. Perdew JP, Ernzerhof M, Burke K (1996) Rationale for mixing exact exchange with density functional approximations. J Chem Phys 105:9982–9985
81. Lindh R, Malmqvist PA, Galgiardi L (2001) Molecular integrals by numerical quadrature. I. Radial integration. Theor Chem Acc 106:178
82. Iliaš Miroslav, Saue Trond (2007) An infinite-order two-component relativistic hamiltonian by a simple one-step transformation. J Chem Phys 126:064102
83. Dyall KG (1994) An exact separation of the spin-free and spin-dependent terms of the Dirac-Coulomb-Breit Hamiltonian. J Chem Phys 100:2118
84. Kutzelnigg W (1984) Basis set expansion of the Dirac operator without variational collaps. Int J Quantum Chem 25:107
85. Hess BA (1986) Relativistic electronic-structure calculations employing a two-component no-pair formalism with external-field projection operators. Phys Rev A 33:3742–3748
86. Wolf A, Reiher M, Hess BA (2002) The generalized Douglas–Kroll–Hess transformation. J Chem Phys 117:9215–9226
87. Reiher M, Wolf A (2004) Exact decoupling of the Dirac Hamiltonian. I. General theory. J Chem Phys 121:2037–2047
88. Reiher M, Wolf A (2004) Exact decoupling of the Dirac Hamiltonian. II. The generalized Douglas–Kroll–Hess transformation up to arbitrary order. J Chem Phys 121:10945–10956
89. Wolf A, Reiher M (2006) Exact decoupling of the Dirac Hamiltonian. III. Molecular properties. J Chem Phys 124:064102
90. Wolf A, Reiher M (2006) Exact decoupling of the Dirac Hamiltonian. IV. Automated evaluation of molecular properties within the Douglas–Kroll–Hess theory up to arbitrary order. J Chem Phys 124:064103
91. Reiher M (2006) Douglass–Kroll–Hess theory: a relativistic electrons-only theory for chemistry. Theor Chem Acc 116:241–252
92. Lévy-Leblond J-M (1967) Nonrelativistic particles and wave equations. Commun Math Phys 6:286
93. AMFI: an atomic mean-field code (1996) B. Schimmelpfennig, Stockholm, Sweden
94. Hess BA, Marian CM, Wahlgren U, Gropen O (1996) A mean-field spin-orbit method applicable to correlated wavefunctions. Chem Phys Lett 251:365–371
95. Visscher L, Saue T (2000) Approximate relativistic electronic structure methods based on the quaternion modified Dirac equation. J Chem Phys 113:3996
96. DIRAC, a relativistic ab initio electronic structure program, Release DIRAC10 (2010) written by Saue T, Visscher L, Jensen HJ Aa, with contributions from Bast R, Dyall KG, Ekström U, Eliav E, Enevoldsen T, Fleig T, Gomes ASP, Henriksson J, Iliaš M, Jacob Ch R, Knecht S, Nataraj HS, Norman P, Olsen J, Pernpointner M, Ruud K, Schimmelpfennnig B, Sikkema J, Thorvaldsen A, Thyssen J, Villaume S, Yamamoto S (see http://dirac.chem.vu.nl)
97. Aquilante F, De Vico L, Ferre N, Ghigo G, Malmqvist P-A, Neograd y P, Pedersen TB, Pitonak M, Reiher M, Roos B-O, Serrano-Andres L, Urban M, Veryazov V, Lindh R (2010) Software news and update MOLCAS 7: the next generation. J Comput Chem 31:224–247
98. Sikkema J, Visscher L, Saue T, Iliaš M (2009) The molecular mean-field approach for correlated calculations. J Chem Phys 131:124116
99. Saue T, Visscher L (2003) Four-component electronic structure methods for molecules. In: Wilson S, Kaldor U (eds) Theoretical chemistry and physics of heavy and superheavy elements. Kluwer, Dordrecht, p 211
100. Visscher L, Dyall KG (1997) Dirac-Fock atomic electronic structure calculations using different nuclear charge distributions. At Data Nucl Data Tables 67:2007
101. Dyall KG (2004) Relativistic double-zeta, triple-zeta, and quadruple-zeta basis sets for the 5d elements Hf-Hg. Theor Chem Acc 112:403–409
102. Dyall KG, Gomes ASP (2010) Relativistic double-zeta, triple-zeta, and quadruple-zeta basis sets for the 5d elements Hf-Hg. Theor Chem Acc 125:97–100
103. Dunning TH Jr (1989) Gaussian basis sets for use in correlated molecular calculations. I. The atoms boron through neon and hydrogen. J Chem Phys 90:1007
104. Roos BO, Lindh R, Malmqvist P-A, Veryazov V, Widmark P-O (2005) New relativistic ANO basis sets for transition metal atoms. J Phys Chem A 109:6575–6579
105. Roos BO, Lindh R, Malmqvist P-A, Veryazov V, Widmark P-O (2005) New relativistic ANO basis sets for actinide atoms. Chem Phys Lett 409:295–299
106. Roos BO, Lindh R, Malmqvist P-A, Veryazov V, Widmark P-O, Borin AC (2008) New relativistic atomic natural orbital basis sets for lanthanide atoms with applications to the Ce Diatom and LuF_3. J Phys Chem A 112:11431–11435
107. Dyall KG, Grant IP, Johnson CT, Parpia FA, Plummer EP (1989) GRASP: a general-purpose relativistic atomic structure program. Comput Phys Commun 55:425–456
108. Kim J, Ihee H, Lee YS (2010) Spin-orbit density functional and ab initio study of HgX_n (X = F, Cl, Br, and I; n=1, 2, and 4). J Chem Phys 133:144309
109. Riedel S, Kaupp M, Pyykkö P (2008) Quantum chemical study of trivalent group 12 fluorides. Inorg Chem 47:3379–3383
110. Cremer D, Kraka E, Filatov M (2008) Bonding in mercury molecules described by the normalized elimination of the small component and coupled cluster theory. Chem Phys Chem 9:2510–2521
111. Schwerdtfeger P, Boyd PDW, Brienne S, McFeaters JS, Dolg M, Liao M-S, Schwarz WHE (1993) The mercury-mercury bond in inorganic and organometallic compunds. A theoretical study. Inorg Chim Acta 213:233–246
112. Kaupp M, Dolg M, von Schnering HG (1994) Oxidation state +IV in group 12 chemistry. Ab Initio study of zinc(IV), cadmium(IV), and mercury(IV) fluorides. Inorg Chem 33:2122–2131
113. NIST Chemistry WebBook (version 69, 2008) National Institute of Standards and Technology, Gaithersburg, MD. (Retrieved 14th Oct 2010)
114. Frisch MJ, Trucks GW, Schlegel HB, Scuseria GE, Robb MA, Cheeseman JR, Scalmani G, Barone V, Mennucci B, Petersson GA, Nakatsuji H, Caricato M, Li X, Hratchian HP, Izmaylov AF, Bloino J, Zheng G, Sonnenberg JL, Hada M, Ehara M, Toyota K, Fukuda R, Hasegawa J, Ishida M, Nakajima T, Honda Y, Kitao O, Nakai H, Vreven T, Montgomery JA Jr, Peralta JE, Ogliaro F, Bearpark M, Heyd JJ, Brothers E, Kudin KN, Staroverov VN, Kobayashi R, Normand J, Raghavachari K, Rendell A, Burant JC, Iyengar SS, Tomasi J, Cossi M, Rega N, Millam JM, Klene M, Knox JE, Cross JB, Bakken V, Adamo C, Jaramillo J, Gomperts R, Stratmann RE, Yazyev O, Austin AJ, Cammi R, Pomelli C, Ochterski JW, Martin RL, Morokuma K, Zakrzewski VG, Voth GA, Salvador P, Dannenberg JJ, Dapprich S, Daniels AD, Farkas, Foresman JB, Ortiz JV, Cioslowski J, Fox DJ (2009) Gaussian 09 Revision A.1. Gaussian Inc. Wallingford CT
115. Visscher L (1997) Approximate molecular relativistic Dirac-Coulomb calculations using a simple Coulombic correction. Theor Chem Acc 98:68
116. Kállay M, Surján PR (2001) Higher excitations in coupled-cluster theory. J Chem Phys 115:2945
117. Nataraj HS, Kállay M, Visscher L (2010) General implementation of the relativistic coupled-cluster method. J Chem Phys 133:234109

118. MRCC, a string-based quantum chemical program suite written by M. Kállay. See also Ref. 116 as well as http://www.mrcc.hu/
119. Zhao Y, Truhlar DG (2008) The M06 Suite of density functionals for main group thermochemistry, thermochemical kinetics, noncovalent interactions, excited states, and transition elements: two new functionals and systematic testing of four M06 functionals and twelve other functionals. Theor Chem Acc 120:215. [Erratum: ibid. 119:525 (2008)]
120. MacDonald AH, Vosko SH (1979) A relativistic density functional formalism. J Phys B 12:2977
121. Ramana MV, Rajagopal AK (1981) Inhomogeneous relativistic electron gas: correlation potential. Phys Rev A 24:1689–1695
122. Ramana MV, Rajagopal AK (1983) Inhomogeneous relativistic electron-systems—a density-functional formalism. Adv Chem Phys 54:231
123. Engel E, Keller S, Bonetti A Facco, Müller H, Dreizler RM (1995) Local and nonlocal relativistic exchange-correlation energy functionals: comparison to relativistic optimized-potential-model results. Phys Rev A 52:2750–2764
124. Engel E, Keller S, Dreizler RM (1996) Generalized gradient approximation for the relativistic exchange-only energy functional. Phys Rev A 53:1367–1374
125. Karasiev VV, Ludeña EV, Shukruto OA (2004) Relativistic Dirac-Fock exchange and Breit interaction energy functionals based on the local-density approximation and the self-consistent multiplicative constant method. Phys Rev A 69:052509
126. Mayer M, Häberlen OD, Rösch N (1996) Relevance of relativistic exchange-correlation functionals and of finite nuclei in molecular density-functional calulations. Phys Rev A 54:4775
127. Varga S, Engel E, Sepp W-D, Fricke B (1999) Systematic study of the Ib diatomic molecules Cu_2, Ag_2, and Au_2 using advanced relativistic density functionals. Phys Rev A 59:4288
128. Varga S, Fricke B, Nakamatsu H, Mukoyama T, Anton J, Geschke D, Heitmann A, Engel E, Bastug T (2000) Four-component relativistic density functional calculations of heavy diatomic molecules. J Chem Phys 112:3499
129. Pipek J, Mezey PG (1989) A fast intrinsic localization procedure applicable for *ab initio* and semiempirical linear combination of atomic orbital wave functions. J Chem Phys 90:4916
130. Strange P (1998) Relativistic quantum mechanics with applications in condensed matter and atomic physics. Cambridge University Press, Cambridge
131. Bast R, Heßelmann A, Salek P, Helgaker T, Saue T (2008) Static and frequency-dependent dipole-dipole polarizabilities of all closed-shell atoms up to radium: a four-component relativistic DFT study. Chem Phys Chem 9:445–453
132. Schmidbaur H, Mandl JR, Wagner FE, van de Vondel DF, van der Kelen GP (1976) ESCA and Mössbauer study of compounds of gold in the oxidation states +I, +II, and +III. J Chem Soc Chem Commun 170–172
133. Parish RV (1982) Gold and Mössbauer Spectroscopy. Gold Bull. 15:51–63
134. Takeda M, Takahashi M, Ito Y, Takano T, Bennett MA, Bhargava SK (1990) ^{197}Au Mössbauer spectra of binuclear gold(I) and gold(II) complexes containing bridging cyclometalated arylphosphine or arylarsine ligands. Chem Lett 543–546
135. Bhargava SK, Mohr F, Takahashi M, Takeda M (2001) ^{197}Au Mössbauer spectroscopy studies of some cyclometalated gold dimers. Bull Chem Soc Jpn 74:1051–1053
136. Bennett MA, Mirzadeh N, Privér SH, Takahashi M, Bhargava SK (2009) ^{197}Au Mössbauer spectroscopic studies of cyclometalated gold dimers containing $2-C_6F_4PPh_2$ ligands. Bull Chem Soc Jpn 82:1506–1509